UNIVERSITÀ DEGLI STUDI DI PADOVA

Sede Amministrativa: Università degli Studi di Padova

Dipartimento di Medicina Molecolare

CORSO DI DOTTORATO DI RICERCA IN: BIOMEDICINA
CURRICOLO: MEDICINA RIGENERATIVA
CICLO XXIX

IN-VITRO ANALYSIS OF QUANTUM MOLECULAR RESONANCE EFFECTS ON HUMAN MESENCHYMAL STROMAL CELLS

Tesi redatta con il contributo finanziario di Telea Electronic Engineering S.r.l.

Coordinatore: Ch.mo Prof. Stefano Piccolo
Supervisore: Ch.mo Prof. Maria Teresa Conconi
Co-Supervisori: Dr. Giuseppe Astori
Dr.ssa Eliana Amati

Dottorando: Sabrina Sella

INDEX

Abbreviations

A2M	Alpha-2-macroglobulin
APC	Allophycocyanin
ARHGAP22	Rho GTPase-activating protein 22
BSA	Bovine serum albumin
CD	Cluster of differentiation
cDNA	complementary deoxyribonucleic acid
CO_2	Carbon dioxide
CORO1B	Coronin-1B
cRNA	complementary Ribonucleic acid
CTL	Control
DEG	Differentially expressed gene
DMEM	Dulbecco's modified eagle medium
D-PBS	Dulbecco's phosphate buffered saline
ECD	Electron coupled dye, also called as PE-Texas Red
ECM	Extracellular matrix
EMF	Electromagnetic field
FBS	Fetal bovine serum
FI	Fold increase
FITC	Fluorescein
FN1	Fibronectin
HCl	Hydrogen chloride
HLA-DR	Human leukocyte antigen D related
IPA	Ingenuity Pathway
ISCT	International society of cellular therapies
kHz	Kilohertz
MFI	Median fluorescence intensity
MHz	Megahertz
MMP1	Matrix metalloproteinase 1
mPMS	1-methoxy-5-methyl-phenazinium methyl sulfate
mRNA	messenger Ribonucleic acid
MSC	Mesenchymal stromal cells
PC7	Phycoerythrincyanin 7
PCR	Polymerase chain reaction

PE	Phycoerythrin
PD	Population doubling
PLAT	Tissue-type plasminogen activator
P/S	Penicillin/streptomycin
QMR	Quantum Molecular Resonance
RNA	Ribonucleic acid
RUNX2	Runt-related transcription factor 2
SD	Standard deviation
SEM	Standard error mean
SHC1	SHC-transforming protein 1
SLIT2	Slit homolog 2 protein
SOX9	SRY-box 9
TBP	TATA-box-binding protein
WST-1	sodium5-(2,4-disulfophenyl)-2-(4-iodophenyl)-3-(4nitrophenyl)- 2H tetrazolium inner salt
YWHAZ	14-3-3 protein zeta/delta

Summary

Effects of high frequency electromagnetic fields and electric currents on biological systems, in particular concerning stem cells, are not extensively studied. Medical devices based on Quantum Molecular Resonance (QMR) technology are actually used in clinical practice for the treatment of musculoskeletal disorders and post-surgical articulation conditions. QMR is a new technology based on the *quantum theory* and assumes that a quantum value of energy exists for breaking every type of molecular bond without any increase of temperature. QMR produces waves at high frequencies (4-64 MHz) and low intensity through oscillating electric currents.

This work aimed at understanding how QMR acts on the regenerative capacities of human bone marrow mesenchymal stromal cells (MSC). MSC are multipotent non-hematopoietic cells with peculiar immunomodulatory and angiogenic properties and a supportive role in hematopoiesis. Moreover their capacity to be recruited in damaged tissues and to differentiate in tissues of mesodermal origin, make them suitable for cellular therapy and in regenerative medicine. MSC cultures were exposed to QMR for two cycles of treatment at two different nominal powers (40 and 80) using an experimental medical device supplied and patented by Telea Electronic Engineering S.r.l. (Italy).

QMR treatments maintained MSC identity and function in terms of morphology, phenotype and multilineage differentiation (adipogenesis, osteogenesis and chondrogenesis). Moreover the treatment did not affect cell viability or proliferation and preserved their intrinsic migration capacity. Microarray analysis revealed that QMR stimulation at 40

nominal power was likely more effective than 80 in inducing molecular changes, as demonstrated by the greater number of up- and down-regulated genes. Specifically, it was observed that genes modulated at 40 were involved into cellular and tissue regeneration processes like extracellular matrix (ECM) remodeling, angiogenesis, cellular migration and regulation of actin filaments. In this regard, quantitative real time PCR results confirmed expression of MMP1, PLAT and A2M genes. These genes generate transcripts for secreted proteins and are involved in ECM remodeling through the fibrinolytic system, which is also implicated in embryogenesis, wound healing and angiogenesis.

We conclude that QMR stimulation might favor tissue regeneration probably supporting neoangiogenesis. Further studies are needed to evaluate how these proteins are implicated in MSC regenerative response after QMR exposition.

Riassunto

Gli effetti dei campi elettromagnetici e delle correnti elettriche ad alta frequenza sui sistemi biologici, in particolare nei confronti delle cellule staminali, non sono stati ancora studiati in modo approfondito. Strumentazioni mediche che si basano sulla tecnologia della Risonanza Quantica Molecolare (QMR) sono attualmente utilizzate nella pratica clinica per trattare patologie muscolo-scheletriche e traumi post-chirurgici alle articolazioni. La QMR è una nuova tecnologia che si basa sulla *teoria dei quanti* ed assume che esiste un valore quantico di energia capace di rompere ogni tipo di legame molecolare senza produrre un incremento di temperatura. La QMR genera onde ad alta frequenza (4-64 MHz) e a basse intensità mediante correnti elettriche oscillanti.

Questo lavoro è focalizzato nella comprensione dei meccanismi alla base dell'azione della QMR sulle capacità rigenerative di cellule mesenchimali stromali (MSC) umane ottenute da midollo osseo. Quest'ultime sono cellule multipotenti non ematopoietiche con peculiari proprietà immunomodulanti e di supporto all'ematopoiesi ed alla neoangiogenesi. In virtù della proprietà di queste cellule di essere reclutate in presenza di un danno tissutale, esse trovano applicazione in protocolli di terapia cellulare e medicina rigenerativa.

Le colture di MSC sono state esposte a due cicli di trattamento con QMR applicando due diversi settaggi noti come potenze nominali 40 e 80, mediante l'uso di uno strumento medico sperimentale fornito e patentato dalla Telea Electronic Engineering S.r.l. (Italia).

In questo studio abbiamo dimostrato che il trattamento con QMR conserva l'identità e la funzione delle MSC in termini di morfologia, fenotipo e

capacità di differenziare in tessuto adiposo, osseo e cartilagineo. Inoltre la stimolazione non altera la vitalità o la proliferazione delle cellule e mantiene la loro intrinseca capacità migratoria.

L'analisi mediante microarray ha suggerito una maggiore efficacia della stimolazione alla potenza nominale 40 nell'indurre cambiamenti a livello molecolare, come dimostrato dal maggior numero di geni up- e down-regolati. In modo specifico, è stato osservato che i geni modulati con il settaggio 40 sono coinvolti nei processi di rimodellamento della matrice extracellulare, angiogenesi, migrazione cellulare e regolazione dei filamenti actinici. Infine risultati ottenuti in real time PCR quantitativa hanno confermato l'espressione dei geni MMP1, PLAT e A2M. Questi geni producono trascritti per proteine secrete e sono coinvolti nel rimodellamento della matrice extracellulare attraverso il sistema fibrinolitico, il quale è implicato nell'embriogenesi, nella guarigione delle ferite e nell'angiogenesi.

In conclusione, la stimolazione con QMR potrebbe favorire la rigenerazione tissutale coinvolgendo probabilmente vie di segnale implicate nella neoangiogenesi. Successivi studi saranno necessari per valutare in modo approfondito come queste proteine possano essere implicate nella risposta rigenerativa delle MSC dopo esposizione con QMR.

1. Introduction

1.1 Definition of electric and electromagnetic fields

Electric field is a vector field caused by stationary electric charge and creates an electric current when modifies spatially through a flow of electric charges. Electric field is always associated with a magnetic field that changes over time and that is well described by Maxwell's equations. The combination of two fields perpendicular to each other, generates an electromagnetic field (EMF). Its propagation form is represented by electromagnetic waves which move out into space and compose the electromagnetic radiation consisting of photons. In other words electromagnetic radiation exhibits both wave and particle properties at the same time.

Electromagnetic radiations are classified in the electromagnetic spectrum (Figure 1) in relation to their frequency (f), that is inversely proportional to wavelength (λ) and directly proportional to photon energy (E), following the formulas: $f = c / \lambda$ and $E = f \cdot h$, where (c) is speed of light in a vacuum and (h) is Planck's constant.

For several decades the diffusion of these fields, as a consequence of advances in technology, has been in depth discussed regarding the safety and degree of their influence in everyday life. In fact we are exposed to increasing numbers of EMFs including extra low-frequency EMFs from electric power lines, EMFs from cell phones and microwaves and many EMFs at mid-range frequencies like house appliances and remote controls.

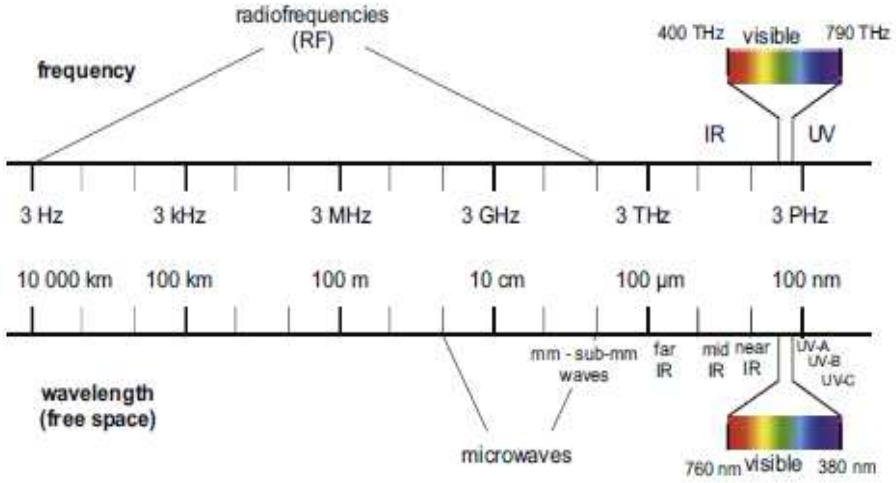

Figure 1. Electromagnetic spectrum. The electromagnetic spectrum covers different frequencies including visible light. Radio frequency (3 Hz - 300 GHz) wavelengths are named originally based on their use in technology for radio communication and broadcasting. However, radio frequencies are used for many other applications nowadays, for example in medical treatments in the range extending from 3 kHz to 300 GHz. Image obtained by Cifra et al. 2011 [1].

The effects of electromagnetic radiation upon biological systems depend indeed both from the radiation's power and its frequency. Generally, radiations can be divided in 2 categories: ionizing and non-ionizing radiations. The first one is composed by ultraviolets, X-rays and gamma rays. They have the ability to cause chemical reactions and damage on living cells because they have enough energy to ionize molecules or affect chemical bonds. The second one consists in radio waves, microwaves, infrared and visible light. Damages inflicted to cells and other materials are determined mainly by power and by heating effects generated from combined energy transfer of photons.

1.2 Interaction with biological systems

Biological systems are composed by heterogeneous components as water, ions, soluble and insoluble molecules, macromolecules like proteins and membranes that have characteristic structures, sizes and properties. All of these components staying in an aqueous environment show a different distribution of charges correlated to their function and play an important role in the biological effects. For this reason their structure can generate endogenous electric currents and EMFs, make them susceptible to external stimulation [2]. In fact the change of charge gradients creates currents inside the cells and initiates mechanisms of interaction and organization at various levels promoting different cellular pathways [3; 4]. In particular it is the case of cellular polar structure like cellular membranes, transport ion channels and cytoskeleton [5-7].

Cellular membranes are no homogenous structures sensible to alterations in the transmembrane potential. The latter is established by the balance of intracellular and extracellular ionic concentration that generates voltage differences influencing transmission of both electrical and chemical signals across membranes to other tissues. Electric fields affect the selective transport of ions or molecules through the membrane changing the accumulation of charged ions layers at the surface (Figure 2) and the manner through which new molecules are incorporated or bound to membrane surface [8]. In the same manner cellular cytoskeleton and its complex structures are good candidates to respond at EMFs and electric currents. They are composed by heterodimeric highly polar subunits that are characterized by a perpetual assembly and disassembly. In particular, microtubules are capable of vibrations in kHz to GHz regions [1] becoming susceptible to eventually structure modification at this

frequency range. In addition Lee and co-workers [7] demonstrated that in the presence of an alternating current electric field, the direction of movement of actin filaments, on myosin coated substrate, is perpendicularly toward the electrode edges and that the alignment is frequency-dependent.

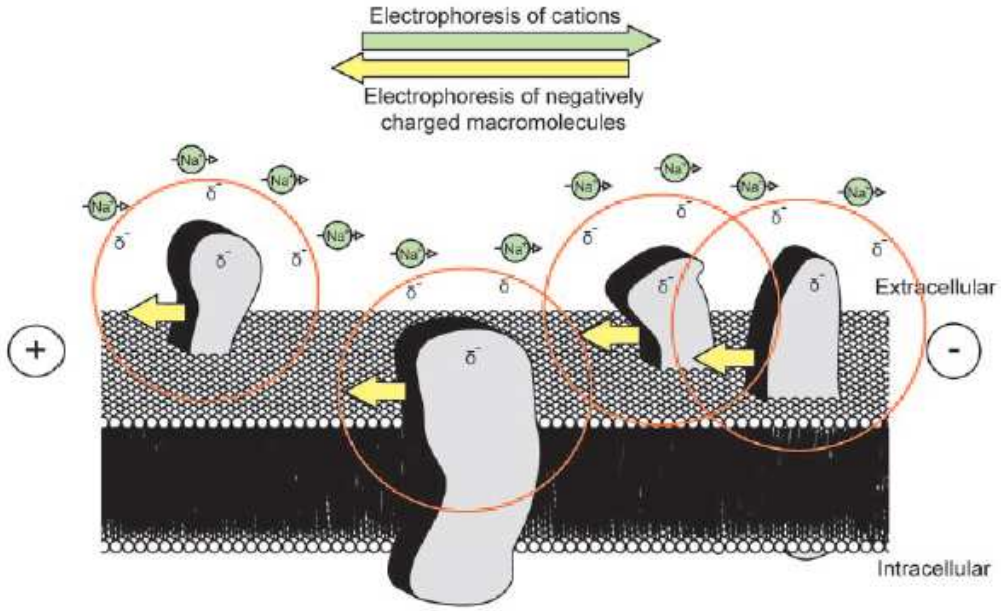

Figure 2. Generation of electrophoresis force on charged species. Macromolecules with negative surface charge are forced toward the anode, while highly extracellular cations, as Na^+, are forced toward the cathode. Arrows indicate the direction of the electrical force on charged species. Circles around proteins signify relative negative charge distribution. Image obtained by Messerli and Graham 2011 [9].

All of these factors play an important role in cellular pathways and tissue physiology demonstrating a therapeutic potential [4]. For this purpose a lot of aspects are studied after EMFs and electrical stimulation with differences in response related to the type of frequency range, particularly at low frequencies, and cellular models. They include promotion and

inhibition of cellular proliferation [10; 11], cellular viability to value adverse outcomes after treatments [12; 13], differentiation [14-16], cellular migration and motility [17-19], inflammatory response [20; 21] and gene expression profiles [22; 23].

1.3 Therapeutic application of electric and EMFs stimulation

1.3.1 Methods and frequencies range of stimulation

Four different modalities have been described to generate electrical fields and EMFs both in-vitro and in-vivo: direct current, capacitive coupling, inductive coupling and combined stimulation [24; 25] (Figure 3).

Direct current is the simplest way of delivering electrical stimulation. It is applied through biocompatible electrodes which are directly connected to tissue or cell culture medium [26]. The use of this method allows control of electrical field in-vitro, but shows concomitant disadvantages. The direct contact between electrodes and cell medium can generate reactions as radical production or electrolysis and can introduce biological active ions that influence cells. This phenomenon makes difficult to separate the real effect due to direct currents by artifacts [27].

Capacitive coupling technique is created between two parallel layers that are placed above and below the culture medium with a non-conductive layer or air gap between them [28]. Its main advantages, consisting in avoiding the issues generated with direct current, can be limited by the high voltages required, which increase with the distance between electrodes.

Inductive coupling approach is the most common method for applying electrical fields in-vivo and in-vitro. It is a non-invasive method consisting of a current-carrying coils which generates an EMF in the proximity of the targeted cells. There are numerous signal configurations concerning this stimulation modality and one of more common subtypes is known as pulsed electromagnetic field stimulation [29], where the stimulus is delivered in pulses and not continuously.

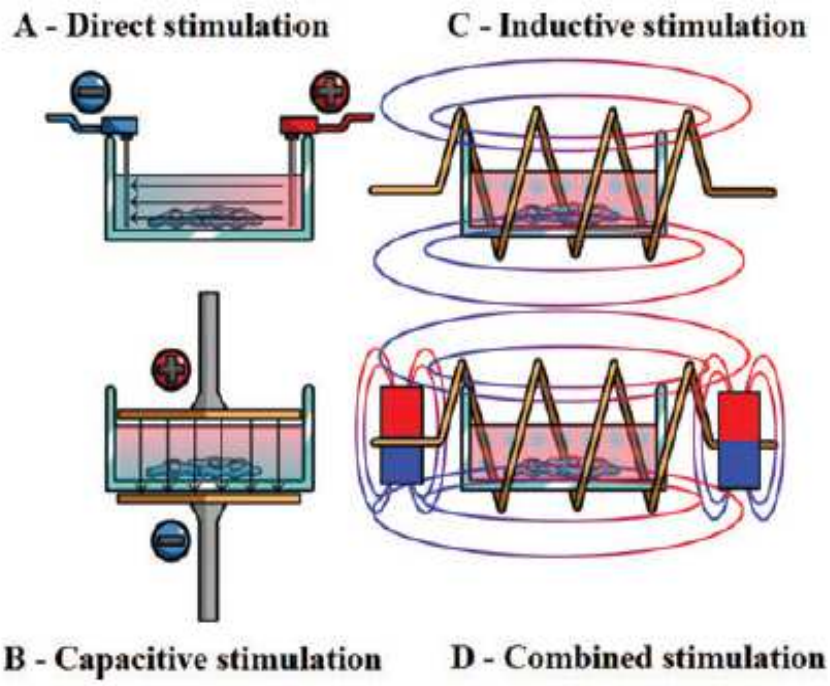

Figure 3. The four main techniques of delivering electrical stimulation. They are the direct (A) and the indirect capacitive (B), inductive (C) and combined (D) methods**.** The latter is a combination of a static magnetic and an alternating current generated by a transient electromagnetic field. Image obtained by Balint et al. 2012 [25].

As reviewed by Markov [30], the therapeutic modalities of stimulation are also based on six groups depending by frequency:

- static/permanent magnetic fields created by permanent magnets or by passing direct current through a coil;
- low frequency sine waves with frequency of 50-60 Hertz;
- pulsed electromagnetic fields at low frequency with specific wave shapes and amplitude;
- pulsed radiofrequency fields in the radiofrequency range (13.56, 27.12 and 40.68 MHz);
- transcranial magnetic/electric stimulation with short pulses (≤8 Tesla);
- millimeter waves at very high frequency range (30-100 GHz).

1.3.2 Clinical applications

In the last years the attention regarding the therapeutic application of EMFs and electric treatments in biomedical field and in regenerative medicine has undergone a huge raise. Several experiments support a role of electric fields in the stimulation of wound healing in frog nerula, salamander skin and mammalian cornea [31]. In particular, manipulation of electromagnetic environment seems to favors wound healing process, reduction of inflammatory state, angiogenesis and extracellular matrix (ECM) synthesis in humans [32]. By contrast, the mechanisms by which the fields improve healing are not known, complicating the use of any specific form of electrical stimulation and the optimization of the treatments [9]. For example EMFs are used in clinic in therapies for cutaneous ulcers with conflicting results. Some studies [33] described that patients affected by leg chronic varicose ulcers were treated using EMFs at very low frequencies during 15 minutes twice a week. In this case significant differences were not revealed in respect to patients that

received a conventional therapy, not considering a decrease in measure of wounds and in circumference of leg. By contrast, Canedo-Dorantes and co-workers [34] reported that, after EMFs treatments for 2-3 hours each day three times a week, 69% of wounds healed and more than 50% of patients healed in 4 months.

Moreover, electrical and EMFs stimulation has been used for the treatment of bone disorders for many years as adjunctive therapy to promote bone healing [35]. It is clinically beneficial for bone fracture healing, treatment of osteoarthritis and pain reduction [35; 36]. Additional experimental studies confirm that EMFs stimulate osteogenesis, increase bone mineral density and decrease osteoporosis [37]. On the other hand a meta-analysis performed by Aleem et al. 2016 [35] suggests that the clinical evidence to support the use of electrical stimulators for bone healing has been inconclusive.

1.4 Quantum Molecular Resonance theory and its related technology

1.4.1 Quantum Molecular Resonance theory

The theoretical basis of Quantum Molecular Resonance (QMR) assumes that a quantum value of energy is able to break every type of molecular bond without increasing of kinetic energy of hit molecules that induces rise in the temperature [38].

The quantum of electromagnetic wave owns energy equal to $E = h \cdot f$, where (h) is Planck's constant and (f) is frequency of wave. According to

Quantum Physics, a system absorbs energy by "packets" also called quanta energy. Consequently a molecular bond can absorb this type of energy where the amount depends by frequency of the wave. In other words the required quanta energy for breaking a molecular bond has to be equal, i.e. in resonance, to the energy of that bond (E*m*) following the formula: E*m* = *k* x *f*, where (*k*) is a constant that depends from the type of the wave and (*f*) is the frequency of wave.

The efficiency of QMR, meaning the capacity of breaking the major number of chemical bonds, is based on the induction of more frequencies producing different quantum energies. QMR generators deliver no ionizing waves at high frequencies (4-64 MHz) and low intensity through alternating electric currents.

1.4.2 QMR related technology

QMR technology has been translated into medical devices by Telea Electronic Engineering S.r.l. (Sandrigo, VI, Italy).

The molecular resonance scalpel Vesalius® is used in surgical purposes for cutting tissues and/or for contemporary coagulation to block bleeding [39; 40]. They are generated by rising of temperature (approximately 63°C) of tissues without necrosis plug and produced by energy concentrated on the tip of scalpel.

The medical device Rexon-age® is adopted for improving post-traumatic tissue regeneration and exploits an elevated power density distributed on the surface of the electrodes adhering to the areas of interest. Today this device is mainly used in clinic for the treatment of musculoskeletal

disorders (inflammations, muscle tears and joint pains) and post-surgical articulation conditions [41; 42].

1.4.3 Previous study of QMR effects on muscle fibers

Dal Maschio and colleagues [43] provide the first description of the behavior of muscle fibers exposed to QMR. They observed that high power stimulation produced a fast and well localized cut of the fibers and that low power stimulation caused a reversible deformation of the membrane. This deformation was accompanied by a membrane depolarization and an increase of cytosolic free calcium, which were detected by fluorescent probes. Both the changes of membrane potential and the variations of free calcium concentration strictly followed the time course of electrical field application and removal.

1.5 Mesenchymal stromal cells

Mesenchymal stromal cells (MSC) are multipotent non-hematopoietic cells. MSC can be isolated from different adult and fetal tissues as bone marrow, umbilical cord, placenta, adipose tissue and synovial fluid. Dominici and co-authors [44] have established minimal criteria to define MSC: plastic adherence, specific surface antigen expression and multipotent differentiation potential in-vitro with adequate culture condition into adipocytes, osteocytes and chondrocytes. Recently this definition has appeared restrictive implicating the need of new approaches for the nomenclature, definition and characterization of MSC [45]. MSC have obtained relevant attention for their particular properties

(Figure 4) such as secretion of trophic and paracrine factors [47], regulation of immune response, anti-apoptotic effects and angiogenesis [48] and capacity to be recruited in damaged tissues [49; 50]. Most of these functions are the result of an induced response to tissue or cell culture environment. For example MSC need to be 'primed' by inflammatory cytokines to become immunosuppressive [51] or mechanically stimulated to create an angiogenesis-promoting environment [52].

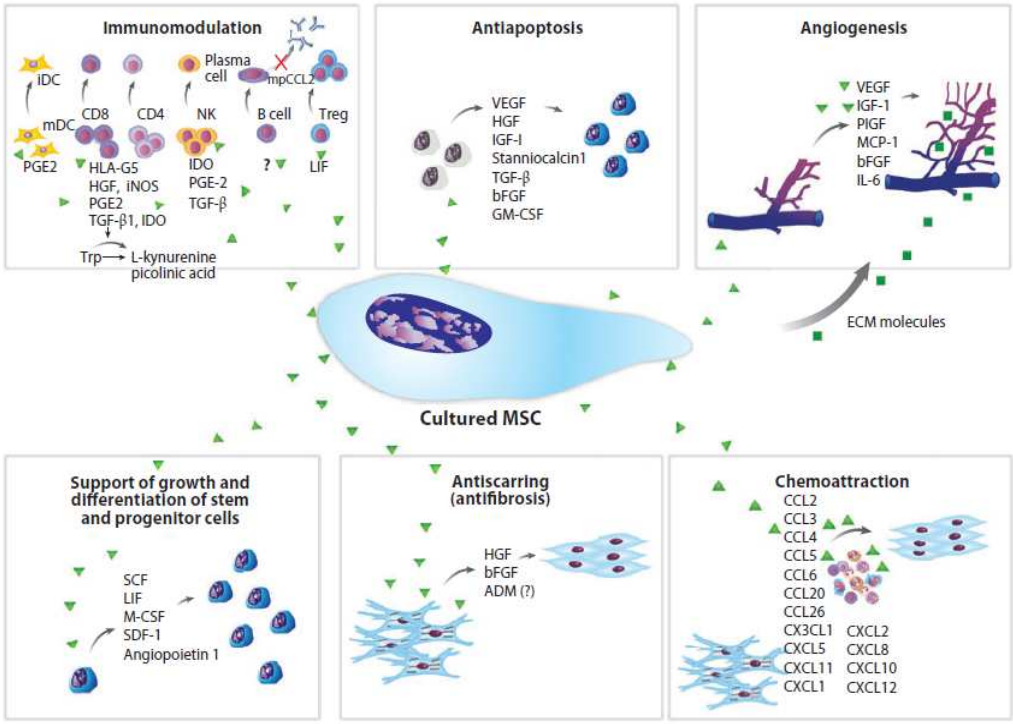

Figure 4. Paracrine effects of cultured MSC. This mechanism can be divided into six main actions: immunomodulation, anti-apoptosis, angiogenesis, support of the growth and differentiation of local stem and progenitor cells, anti-scarring and chemoattraction. Image obtained by Singer et al. 2011 [46].

The availability and versatility of MSC make them an excellent treatment option for a wide variety of clinical settings [53]: from orthopedics and

spine therapies, to cardiovascular therapies, wound care and soft tissue repair, neural disorders, spinal cord injury and autoimmune disorders. Accumulated data indicate that MSC support healthy physiologic functioning towards successful healing, suggesting a role in all the three phases of wound healing represented by inflammation, proliferation and remodeling [54].

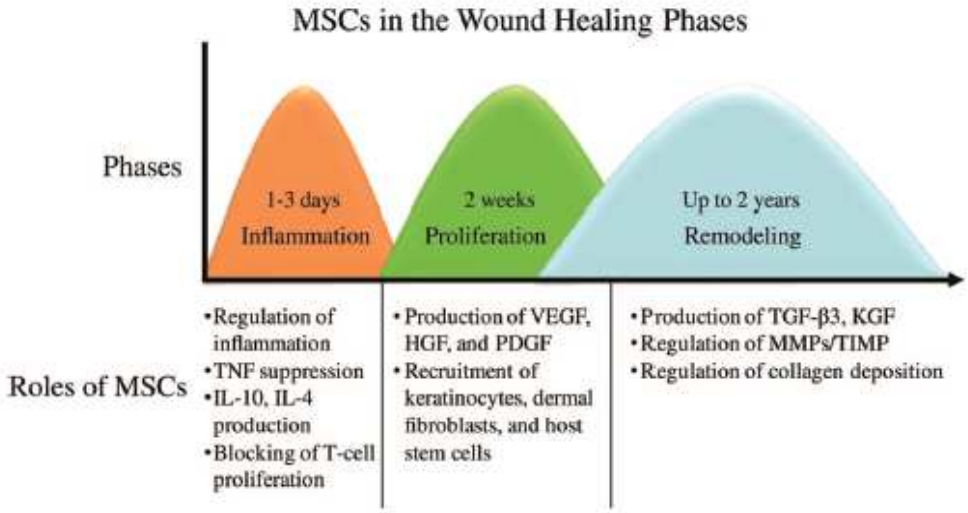

Figure 5. MSC roles in each phase of the wound healing process. Image obtained by Maxson et al. 2012 [54].

As illustrated in Figure 5, MSC promote the transition from inflammatory to proliferative phase, particularly critical for treating chronic wounds where high levels of inflammation prevent healing. MSC also contribute to proliferative phase by expressing growth factors as vascular endothelial growth factor (VEGF), hepatocyte growth factor (HGF), and platelet-derived growth factor (PDGF) to promote epithelialization. Finally, MSC regulate remodeling of healed wound through the regulation and organization of ECM deposition. Badiavas and colleagues [55]

demonstrated that MSC can be successful in the treatment of non-healing chronic wounds. In similar way in a clinical randomized study [56] on 24 patients with non-healing ulcers, the implant group had significant improvement in pain-free walking distance and reduction in ulcer size after 12 weeks.

2. Aim

Medical devices based on QMR technology are actually used for the treatment of musculoskeletal disorders and post-surgical articulation conditions [41; 42].

Effects of high frequency EMFs and electric currents on biological systems, in particular concerning stem cells, are not extensively studied.

QMR exploits high frequency waves between 4 and 64 MHz at low intensity delivered through alternating electric currents. Because few data are available from the literature on this technology and on QMR frequency range, our work was focused on understanding how QMR acts on the regenerative capacities of human bone marrow-derived MSC. These latter represent a promising cell-based therapeutic approach in regenerative medicine [49]. In particular it was demonstrated that endogenous bone marrow-derived MSC were recruited and mobilized to sites of injury [57] suggesting the importance of studying QMR exposition on this cell type.

This study evaluated the effects of QMR on the identity and function of MSC. In first instance, we have investigated *in-vitro* MSC morphology, phenotype, multi-differentiation potential, viability, cellular proliferation and migration. Moreover, we analyzed at a molecular level relevant pathways possibly involved in QMR effects, by using microarray technology and quantitative real time PCR.

MSC cultures were exposed to QMR using an experimental medical device supplied and patented by Telea Electronic Engineering S.r.l. (Italy).

3. Materials and methods

3.1 Isolation and culture of MSC

MSC were isolated starting from human bone marrow washouts of discarded bags and filters used for allogeneic transplantation. The procedure was approved by the ethics committee of San Bortolo Hospital, Vicenza, Italy. After 2 washing steps with 200 ml saline solution and centrifugation at 2.000 rpm for 10 min, whole unprocessed total nucleated cells were seeded *in toto* at the density of $1x10^5$ cells/cm^2 in low-glucose Dulbecco's modified Eagle's medium (DMEM) with GlutaMAX™ and pyruvate (Gibco, Thermo Fisher Scientific), supplemented with 10% fetal bovine serum (FBS, Qualified Australian, Gibco, Thermo Fisher Scientific) and 1% penicillin/streptomycin (P/S, Sigma-Aldrich). Cultures were incubated at 37°C in a humidified atmosphere with 5% CO_2. Non-adherent cells were removed after 72 hours and fresh medium was added, then culture medium was changed every 3-4 days. At 80% confluence, MSC were washed with Dulbecco's phosphate buffered saline (D-PBS, Sigma-Aldrich), harvested using 10X TrypLE Select (Gibco, Thermo Fisher Scientific) and sub-cultured at a density of 1500 cells/cm^2. For QMR experiments, MSC samples were seeded in 35 mm-diameter Petri dishes (CELLSTAR®, Greiner Bio-One) and passage numbers 4-6 were used.

The cultures were observed with an inverted light microscope Axiovert 40 CFL (Carl Zeiss) and the images acquisition obtained by AxioCam Mrm camera system (Carl Zeiss).

3.2 QMR stimulation protocol

MSC cultures were exposed to QMR using an experimental medical device supplied and patented by Telea Electronic Engineering S.r.l. (Italy). The prototype worked with the following parameters:

- Alimentation: 230 V ~ 50/60 Hz;
- Maximum power in input: 250 VA;
- Power in output: 45 W/400 Ω.

The rise of effective powers delivered in output corresponded to increase in value of the nominal powers employed as QMR settings. In detail, the prototype enhanced alternating electric currents characterized by high frequency waves and low intensity, where the fundamental wave was at 4 MHz and the subsequent ones increased in harmonic content until 64 MHz.

The exposure system was composed by a pair of custom made sterilized spheroidal electrodes of 35 mm-diameter and by a metallic plate. The electrodes were collocated inside 2 different Petri dishes and supported by polyvinyl chloride (PVC) component to allow the direct contact with the surface of culture medium. The metallic plate was positioned externally to the bottom of Petri dishes (Figure 6 A).

After 72 hours from initial seeding, complete medium was changed. MSC cultures were undergone at 2 QMR cycles of stimulation, for 10 minutes/day for 4 consecutive days (Figure 6 C). Cells were treated at 2 different QMR settings corresponding to 40 and 80 nominal powers, with each condition performed in duplicate (Figure 6 B).

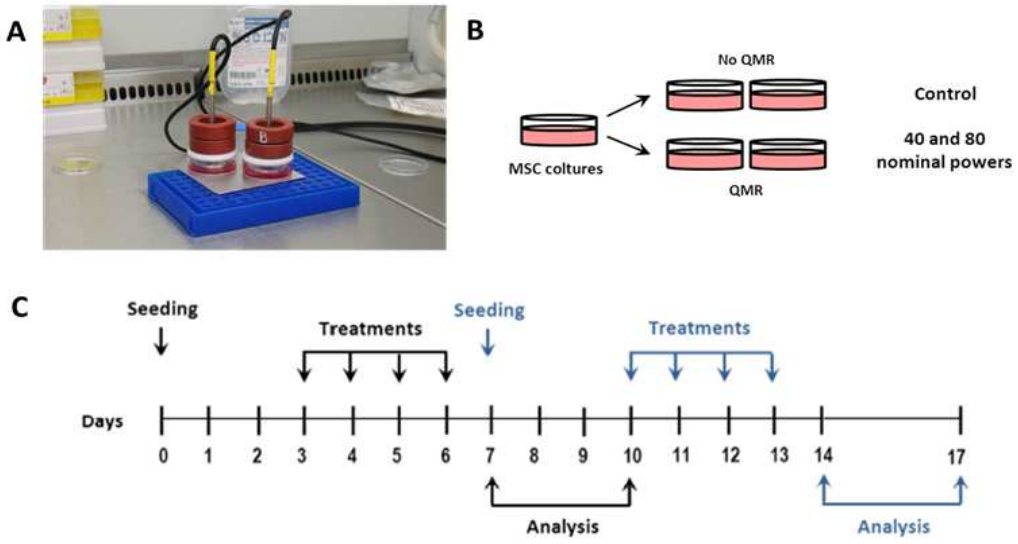

Figure 6. QMR stimulation protocol. A) Image of exposure system. B) and C) Scheme of QMR treatment. Cells were seeded on day 0, harvested and reseeded on day 7. The first cycle of treatment started on day 3 (black arrows), the second one on day 10 (blue arrows), 10 minutes/day for 4 consecutive days at 40 or 80 nominal powers. Sham-exposed controls were kept in parallel.

3.3 MSC phenotype characterization

MSC phenotype was characterized by flow cytometry before and after QMR stimulation. Briefly, $1x10^5$ cells were incubated with the following monoclonal antibodies: CD90-FITC (clone F15-42-1-5), CD105-PE (clone 1G2), CD45-ECD (clone J.33), HLA-DR-APC (clone IMMU 357) (all purchased from Beckman Coulter) and CD73-PC7 (clone AD2) (Becton Dickinson) for 15 minutes protected from light at room temperature. After a wash with D-PBS to eliminate the surplus of antibodies, cells were suspended in D-PBS with 1% bovine serum albumin (BSA, Miltenyi Biotec). At least 20.000 cells were acquired on a FC500 flow-cytometer (Beckman Coulter) and data were analyzed by Kaluza software (Beckman

Coulter). The expression of each marker was assessed as percentage (%) of positive cells and as fold increase (FI), this latter defined as the ratio between the median fluorescence intensity (MFI) of the marker and its specific negative control.

3.4 Multilineage differentiation

After two cycles of consecutive stimulations the maintenance of MSC differentiation potential was tested. Samples were harvested and re-seeded in 24-well plates (Falcon®, Corning Life Sciences) in presence of sterile circular coverslips (13 mm-diameter and 0.2 mm-thickness, Thermo Scientific Nunc) at the density of 4.000 cells/cm^2. Differentiation was induced at semi-confluence with specific differentiation media for 21 days (StemPro Adipogenesis kit, StemPro Osteogenesis kit, StemPro Chondrogenesis kit, Gibco, Thermo Fisher Scientific). Fresh medium was added every 3 days and the respectively controls were maintained in parallel with the standard expansion medium (DMEM + 10% FBS + 1% penicillin/streptomycin).

To detect the formation of lipid droplets, cells were fixed in 10% formalin for 5 minutes and stained with Oil Red O (Diapath Spa). Briefly, the samples were incubated for 10 minutes with Oil Red O solution. After abundant washing, the coverslips were covered with 10 drops of Mayer's haematoxylin for 3 minutes and then washed with deionized water.

The presence of calcific deposition as expression of osteogenic induction was analyzed through Alizarin red staining. The samples were washed with D-PBS and fixed in ice-cold 70% ethanol at 4°C for 1 h. Then, they

were incubated for 15 minutes with Alizarin red solution (0.02 g/ml filtered; Sigma-Aldrich) at room temperature. Finally, several washes were performed with deionized water.

To verify chondrogenic differentiation, cells were fixed in 10% formalin for 5 minutes and stained with Alcian blue (1 g/l in 0.1 M HCl) for 2 h at room temperature. At the end of the staining, specific for acidic polysaccharides, the coverslips were rinsed extensively with deionized water.

After each staining, the coverslips were mounted on microscope slides using Kaiser's glycerol gelatine pre-warmed at 37°C. The acquisition of images was obtained by AxioCam Erc 5s camera system (Carl Zeiss).

3.5 Assessment of cellular viability

Cellular viability was determined by flow cytometry using LIVE/DEAD® Fixable Far Red Dead Cell Stain kit (Invitrogen™, Thermo Fisher Scientific). The reactive dye was able to permeate the compromised membranes of dead cells reacting with free amine both intracellularly and on cell surface. This way, dead cells resulted brighter in fluorescence in respect of viable cells (Figure 7).

Briefly, QMR-treated samples were harvested and $1x10^5$ cells were used for the assay. The cellular suspensions were rinsed once with D-PBS and suspended in 100 µl D-PBS. 10 µl of diluted 1:100 dye were added into the suspensions before incubation at room temperature for 30 minutes protected from light. After washing with D-PBS supplemented with 1% BSA, the samples were re-suspended in 100 µl of D-PBS + 1% BSA and

acquired on a FC500 flow-cytometer. Data were analyzed as % of dim or bright positive cells by Kaluza software.

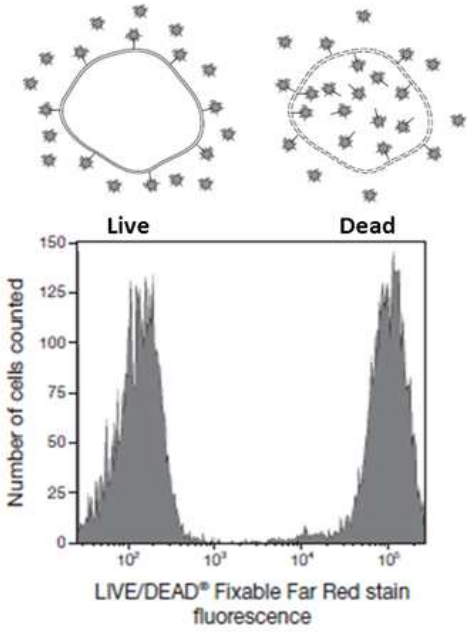

Figure 7. LIVE/DEAD® assay. This assay is based on the reaction between a fluorescent reactive dye and cellular amines. Live and dead cells can be distinguished easily by flow cytometry with a difference in fluorescent intensity typically greater than 50-fold. Image was obtained and modified by manufacturer's guide.

3.6 Quantification of cellular proliferation

QMR effects on cellular proliferation were determined in two ways:

1) measuring the Population Doubling (PD)
2) performing the WST-1 assay (Sigma Aldrich).

PD is an accurate estimation of cell growth that considers the number of duplications of a given population from initial seeding. PD was evaluated using Trypan blue exclusion test and according to the following formula:

PD = [log (*Nf*) – log (*Ni*)] / log 2, where (*Nf*) represents the number of harvested cells and (*Ni*) the number of initially seeded cells.

WST-1 is a tetrazolium negatively charged disulfonated inner salt containing an iodine residue. It is reduced extracellularly to its soluble derivative formazan by electron transport across the plasma membrane of dividing cells via the electron mPMS carrier (Figure 8). The reduction of WST-1 is directly proportional to the number of metabolically activated cells in exponential growth phase [58].

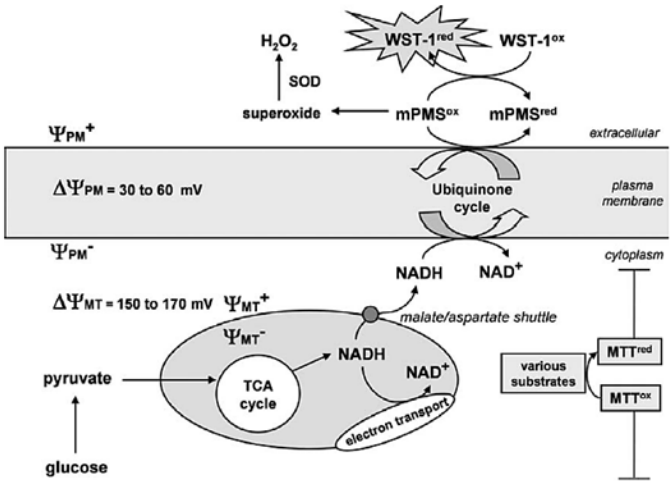

Figure 8. Schematic representation of the reduction mechanism of WST-1. Image extracted from Berridge et al. 2005 [58].

In detail, at the end of 2 consecutive cycles of QMR treatment, samples were harvested, counted with Trypan blue and seeded in 96 well-plates (Falcon®, Corning Life Sciences) at the density of 2000 cells/well in a final volume of 100 µl/well of culture medium with eight replicates per condition. After 72 hours 10 µl/well of the probe WST-1 were added and plates were incubated for 3 hours at 37°C. Finally, the plates were read by

a spectrophotometer (SpectraCount™ Packard) at 450 nm wavelength to measure the absorbance of samples. Data were expressed as % proliferation on the control.

3.7 Scratch test migration assay

Cells were harvested and re-seeded in 24 well-plates at a density of $1x10^4$ cells/well in triplicate conditions. At 100% of confluence, vertical scratches were performed using 1000 µl plastic sterile tips (Sarstedt) to create a gap of about 1 mm. To eliminate dislodged cells, culture medium was removed and wells were washed with 1 ml of DMEM. New complete medium was added. Images of scratches were taken at different time points (Figure 9) and analyzed using Zen pro 2012 software (Carl Zeiss). The results were calculated as: % Closure = [(Area t_0 – Area t_x)/ Area t_0] x 100 , where t_0 represented the initial scratch area and t_x the time course scratch area.

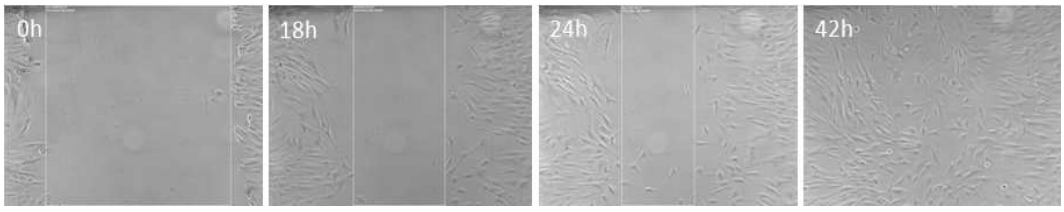

Figure 9. Scheme of scratch test migration assay. A wound was created into a monolayer of confluent MSC culture and the cell-free area was measured at specific time points (0 h, 18 h, 24 h and 42 h).

3.8 Microarray analysis

The RNA derived from 5 different MSC samples exposed to 1 cycle of QMR stimulation were extracted using RNeasy plus mini kit (Qiagen) according to the manufacturer's instructions. The total RNA quantification was obtained with NanoDrop UV-VIS Spectrophotometer (Thermo Fisher Scientific). Microarray analysis was performed in collaboration with High Throughput Screening facility of the Centre for Integrative Biology (CIBIO, Trento, Italy), where the microarray experiments were performed. The quality of RNA was determined using Agilent 2100 Bioanalyzer system with Eukaryote Total RNA Nano kit (Agilent Technologies). The samples were processed according to protocol "Agilent One-Color Microarray-based Gene Expression Analysis (Low Input Quick Amp Labeling)" with Human GE 4x44K V2 Microarray Kit with SurePrint technology (Agilent Technologies) illustrated schematically in Figure 10. Briefly, cDNA was synthesized by 200 ng of RNA in presence of RNA Spike-In (technical probes control) and then transcripted into complementary RNA (cRNA), marked during the reaction with cyanine 3 dye. The cRNAs were purified with RNeasy columns (Qiagen) and fragmented with specific buffers coupled to heat. The hybridization between the samples and the microarray slides was performed for 17 hours at 65°C. After washing steps to remove unspecific binding, the microarray slides were detected with Agilent scanner through ScanControl software. The translation from hybridization signal into numeric format was produced by Agilent Feature Extraction software.

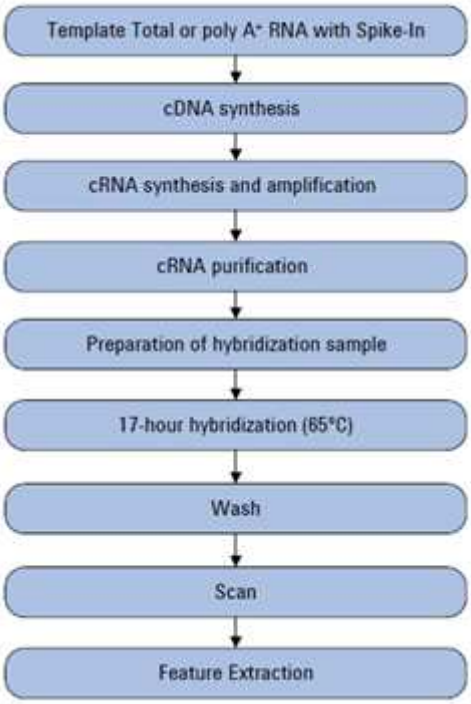

Figure 10. Microarray workflow for samples preparation and arrays procession according to manufacturer's protocol. Image obtained and modified by manufacturer's guide.

Afterward data were subjected to a pre-processing step consisting in 4 phases: background subtraction, normalization, removal of probes according to flag quality and addition of the replicated probes. The quality of signals of hybridization was visualized through MA plot graphics that compared hybridization signals of all probes of one sample in respect of all probes of the other samples. Three out of the 16 samples (15 samples + 1 technical replicate) showed an aberrant hybridization and they were not used for the analysis of the differentially expressed genes this latter elaborated with open-source program Bioconductor [59].

3.9 Quantitative real time PCR

MSC cultures were exposed or not to QMR at 40 nominal power for 1 cycle and the total RNA was extracted using RNeasy Plus Mini Kit (Qiagen) following the manufacturer's instructions. Quality and quantity were determined using Nanodrop UV-VIS Spectrophotometer (Thermo Fisher Scientific). cDNA was synthesized in 20 μl reaction volume with 800 ng of total RNA using the iScript cDNA synthesis kit (Bio-Rad Laboratories) according to the manufacturer's instructions.

The obtained cDNA was diluted 1:10 and the quantitative real time PCR experiments were performed using SsoFast EvaGreen Supermix with Low Rox (Bio-RAD Laboratories) on ABI 7500 Real-Time PCR System (Applied Biosystem, Thermo Fisher Scientific). The investigated genes were shown in Table A and primers used for the amplification were validated and obtained by Bio-RAD Laboratories. The protocol consisted of 30 seconds at 95°C, 40 cycles of 5 seconds at 95°C and 32 seconds at 60°C, followed by a final melting step to evaluate the quality of product. Each gene was tested in three replicates. Data acquisition was obtained by SDS v1.2 software (Applied Biosystem, Thermo Fisher Scientific) and the relative expression was determined using $2^{-\Delta\Delta Ct}$ method [60] with TBP and YWHAZ as reference genes [61].

Gene name	UniGene ID	RefSeq
MMP1	Hs.83169	NM_002421
PLAT	Hs.491582	NM_000930
SLIT2	Hs.29802	NM_004787
ARHGAP22	Hs.655672	NM_021226
A2M	Hs.212838	NM_000014
CORO1B	Hs.6191	NM_020441
SHC1	Hs.433795	NM_183001
FN1	Hs.203717	NM_054034
RUNX2	Hs.535845	NM_001024630
SOX9	Hs.647409	NM_000346
TBP	Hs.590872	NM_003194
YWHAZ	Hs.492407	NM_145690

Table A. List of genes used for quantitative real time PCR experiments. In the table gene name, UniGene database identification code (UniGene ID) and NCBI Reference Sequence Database code (RefSeq) of genes used for quantitative real time experiments with SYBR® Green method were illustrated.

3.10 Statistical analysis

To analyze the differences between the experimental settings and the sham-exposed controls after both QMR cycles, data were analyzed by one-way ANOVA followed by Dunnett's multiple comparison post-hoc test. Quantitative real time PCR data were analyzed by paired t-test comparing the ΔCt values at 40 with the controls. Statistical analysis was performed using GraphPad Prism version 5.01 (GraphPad Software). Differences between samples were considered statistically significant at $p<0.05$.

For microarray data analysis the "R language *limma* package" was used to identify the differentially expressed genes (DEG) [59], with Bayes' empirical method considering the provenience of lots (paired test). Differences between conditions were considered significant after Benjamin & Hochberg correction at $p<0.05$. To analyze the best enrichment of gene lists, the ToppGene Suite and Ingenuity Pathway Analysis (IPA) programs were applied, considering q-value<0.01 with FDR Benjamin & Hochberg correction and p-value<0.01 with Bonferroni-Hochberg correction, respectively.

4. Results

4.1 Analysis of cellular morphology

MSC morphology was observed daily before and after QMR treatments at the different settings. The cells conserved their canonical fibroblast-like spindle-shaped aspect during all the time of the experiments (Figure 11), with no cells in suspension or in semi-adherence that could indicate a QMR induction to cellular death. No other signs of alteration in cell size, multinuclear cells and cytoplasmic granulations were present.

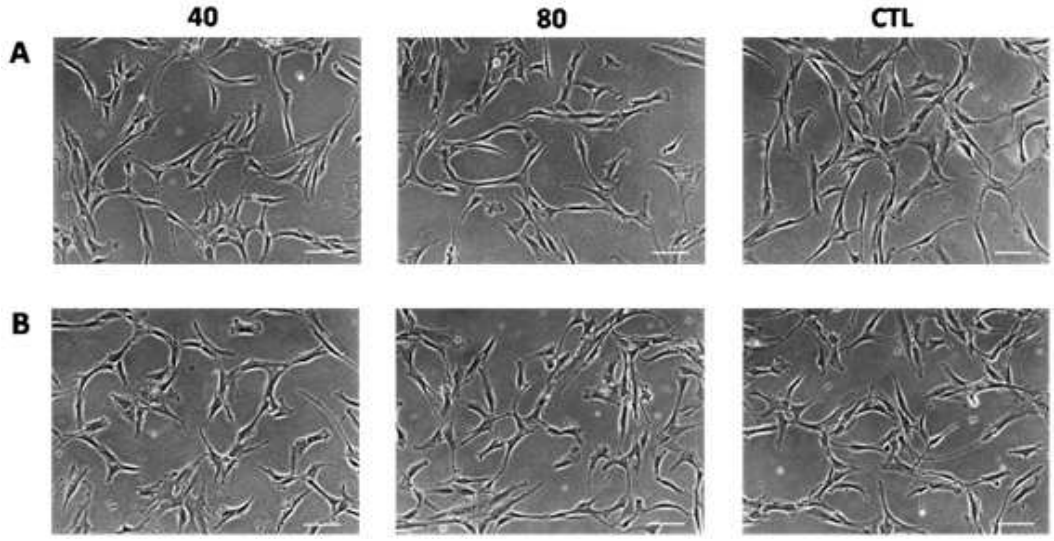

Figure 11. MSC morphology after QMR stimulation. The images were obtained after 10 minutes of QMR stimulation. A) Day 5 (first cycle of treatment); B) Day 12 (second cycle of treatment). Scale bar = 100 μm. Total magnification = 100X. One representative experiment was shown.

4.2 Analysis of MSC surface markers

Phenotypic MSC characterization after the first and second cycle of treatment with QMR was performed by flow cytometry in agreement with ISCT criteria [45]. Particularly, the expression of CD90, CD105 and CD73 on gated MSC was always over 95%, while that of CD45 and HLA-DR constantly lower than 2% (Table B).

As shown in Figure 12, each marker showed inter-batches biological variability without statistical significance between treated and untreated samples after 1 and 2 cycles of stimulation.

% Positive cells	First cycle of treatment			Second cycle of treatment		
QMR setting	**40**	**80**	**CTL**	**40**	**80**	**CTL**
CD90-FITC	99,92 ± 0,09	99,87 ± 0,17	99,87 ± 0,13	99,44 ± 0,49	99,52 ± 0,36	99,48 ± 0,37
CD105-PE	99,98 ± 0,01	99,98 ± 0,02	99,98 ± 0,01	99,79 ± 0,23	99,84 ± 0,15	99,79 ± 0,23
CD73-PC7	99,98 ± 0,01	99,98 ± 0,01	99,99 ± 0,01	99,81 ± 0,20	99,87 ± 0,12	99,80 ± 0,23
CD45-ECD	0,33 ± 0,15	0,31 ± 0,13	0,42 ± 0,34	0,25 ± 0,30	0,28 ± 0,30	0,21 ± 0,20
HLA-DR-APC	2,44 ± 1,82	2,17 ± 1,74	2,11 ± 1,23	1,39 ± 1,02	1,07 ± 0,77	0,97 ± 0,65

Table B. MSC flow cytometry analysis after QMR stimulation at different settings. A five color combination of monoclonal antibodies was used to verify MSC identity according to the above listed surface markers. Data are presented as mean ± SD of 3 independent experiments.

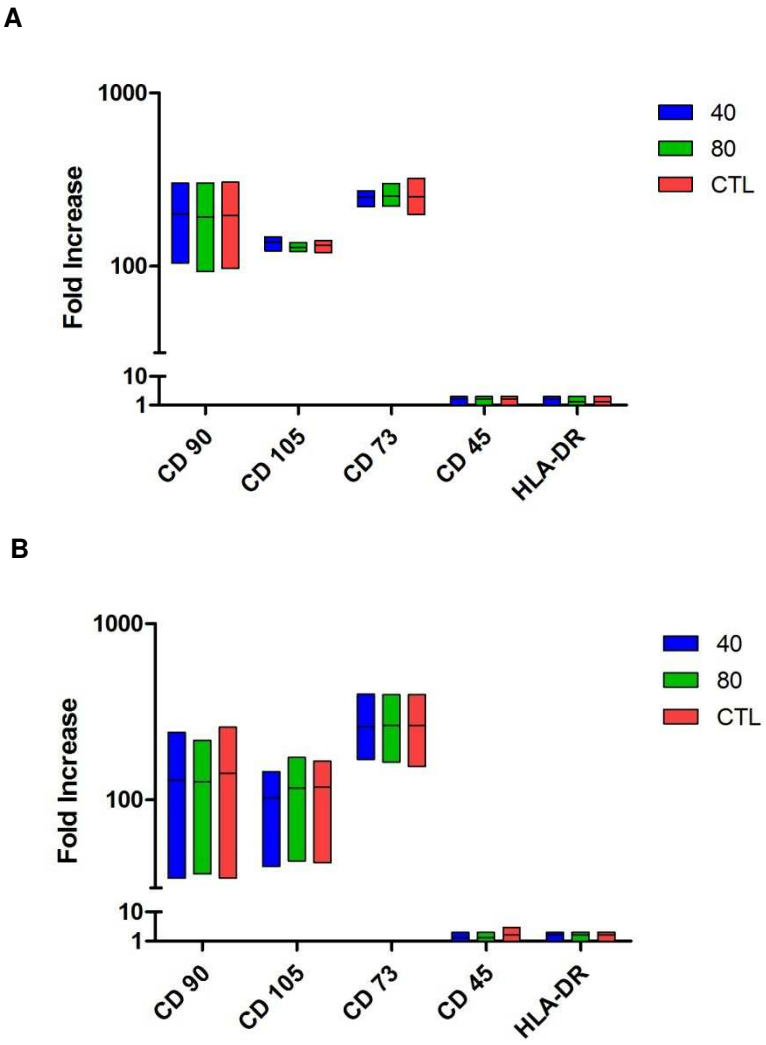

Figure 12. Fold increase of MSC markers after QMR stimulation at different settings. A) First cycle of treatment; B) Second cycle of treatment. Bars represented the maximum, median and minimum values of 3 independent experiments. The y-axis was in log10 scale.

4.3 Analysis of MSC differentiation potential

To investigate the *in-vitro* differentiation potential of MSC after 2 cycles of QMR treatment, cells were induced or not to differentiate down the osteogenic, adipogenic and chondrogenic lineages, by using defined

media components and culture conditions. All samples demonstrated osteogenic, adipogenic and chondrogenic differentiation after 3 weeks of induction, being positive to Alizarin Red, Oil Red O and Alcian blue stainings (Figure 13). No qualitative differences were observed between QMR-treated and non-treated MSC samples. Similar results were observed after 1 cycle of stimulation (data not shown).

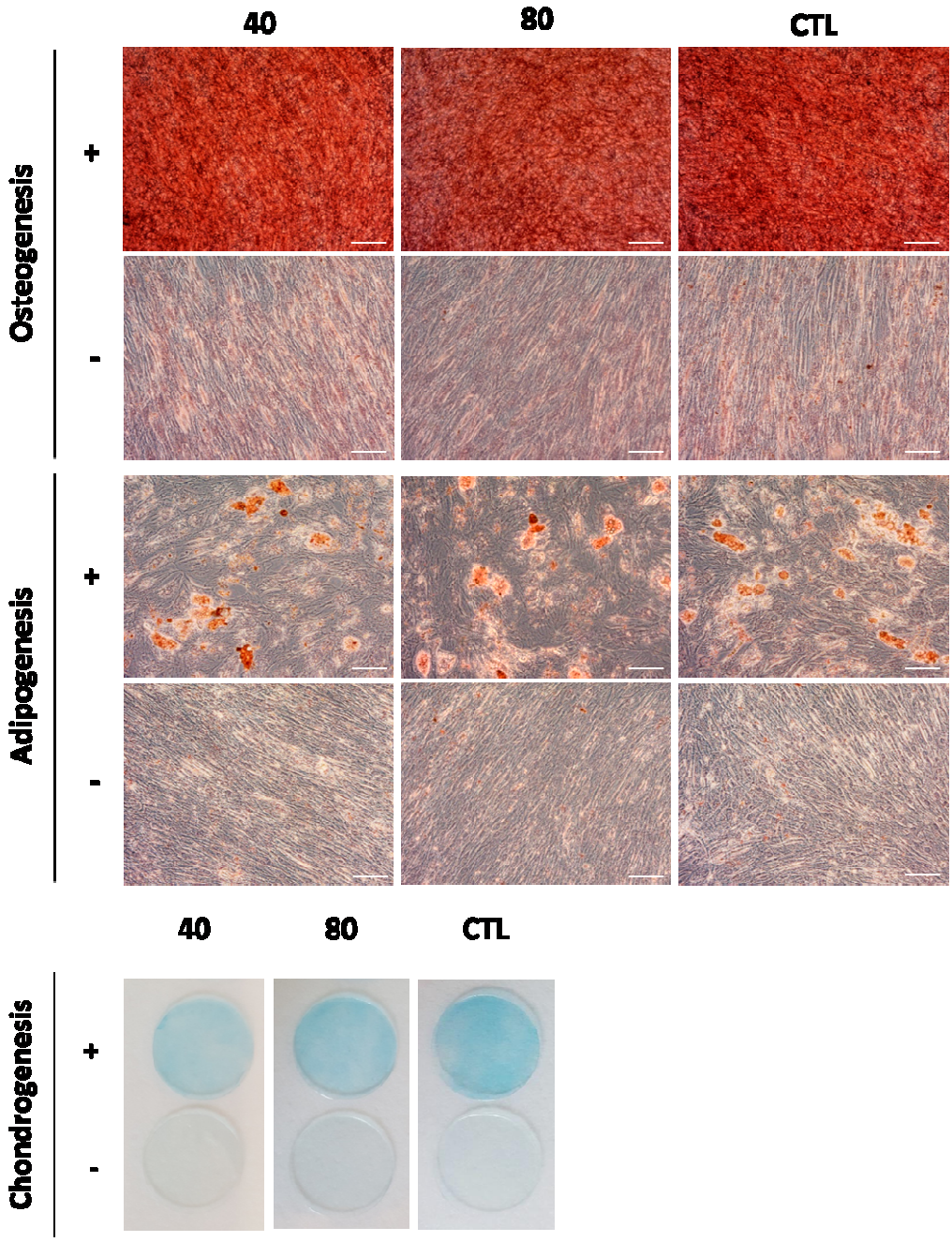

Figure 13. Adipogenic, osteogenic and chondrogenic differentiation after 2 QMR cycles of stimulation. Panels display one representative experiment showing the final outcome in MSC multilineage differentiation after 21 days of induction. QMR-treated (at 40 and 80 nominal powers) and untreated samples (CTL) were induced (+) or not (-) to differentiation. Osteogenic, adipogenic and chondrogenic differentiation were assessed using Alizarin Red, Oil Red O and Alcian Blue stainings, respectively. Scale bar =100 μm. Total magnification = 100x.

4.4 Effect of QMR stimulation on cellular viability

Cellular viability in treated/untreated MSC was quantified by flow cytometry at the end of each cycle (Figure 14). Data showed that viability was not affected by QMR; indeed, more than 95% of cells were alive similarly to the controls, with low variability between the different MSC batches and settings. These results confirmed the morphological observations.

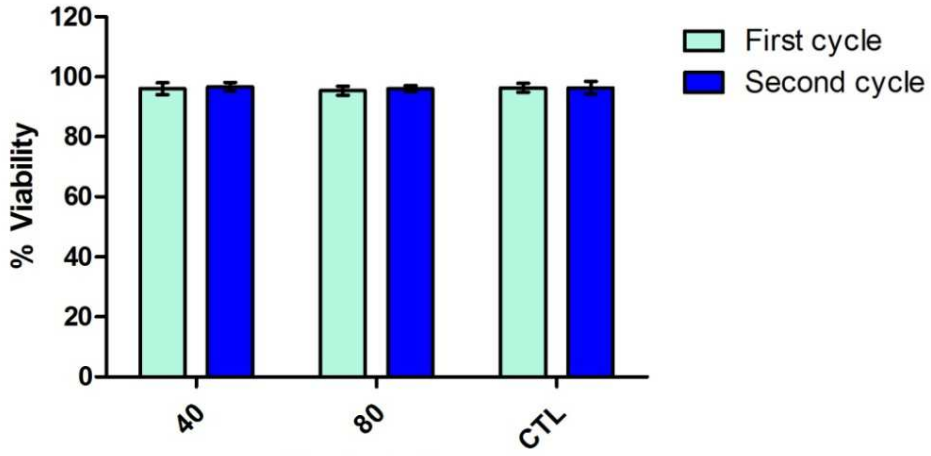

Figure 14. Cellular viability after QMR treatment. Histograms represent the % of cellular viability after two cycles of QMR treatment at the different settings compared to

the sham exposed controls. Data are shown as mean ± SD of 3 independent experiments. No statistical differences were found between conditions.

4.5 Effect of QMR on MSC proliferation

As shown in Figure 15, replication of MSC cultures was not affected by QMR. In detail, our results showed no significant differences in the PD between controls and QMR-treated samples, at the different settings and times (Figure 15, A). In the same way WST-1 assay revealed no significant effects due to QMR exposition. By normalizing all values on the respective controls, mean values were about 101% and 107% of MSC proliferation obtained treating with 40 setting after 1 and 2 cycles, respectively. At 80 setting the percentages of proliferation were 104% and 99%, respectively (Figure 15, B).

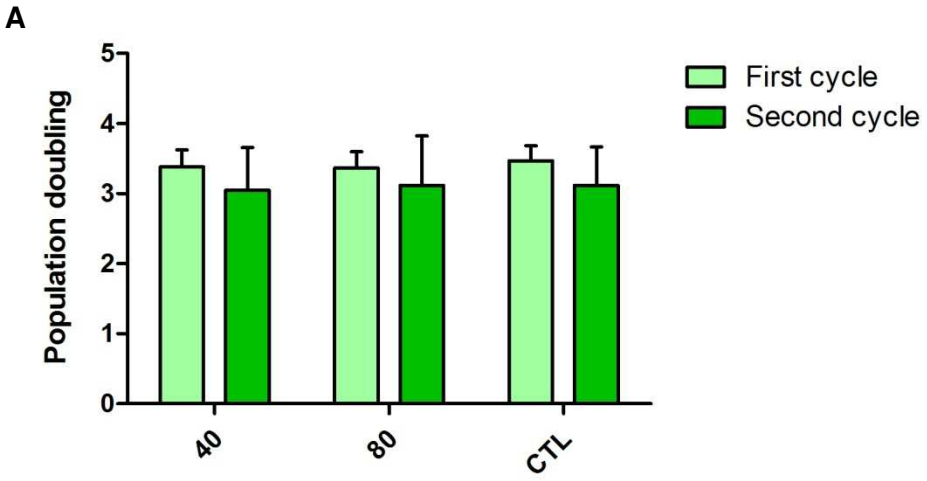

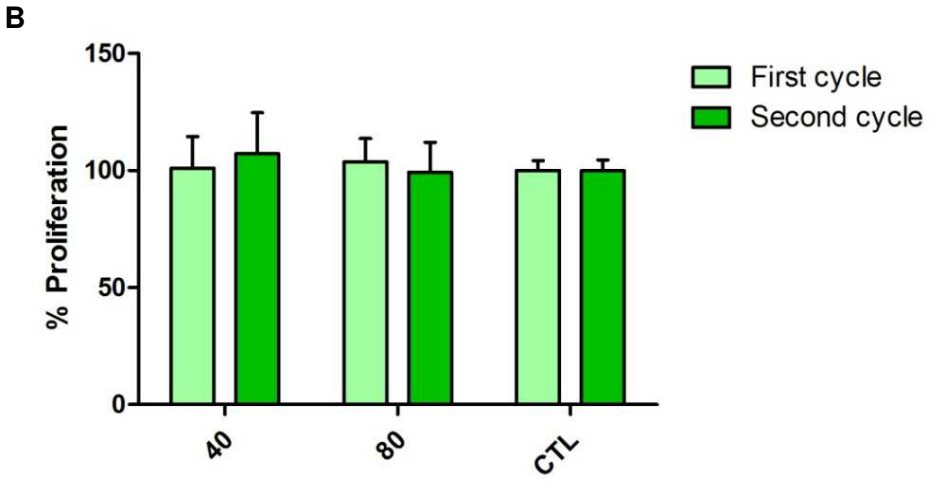

Figure 15. Cellular proliferation after QMR stimulation. A) PD were assessed using Trypan blue exclusion test after the two cycles of QMR at day 7 and 14, respectively; B) Percentages of cellular proliferation on the controls were obtained by WST-1 assay after 72 hours. Data are represented as mean ± SD of n=6 independent experiments.

4.6 Effect of QMR stimulation on MSC migration

QMR treatment after two cycles at the different settings did not modify the migration capacity of MSC. The gap closure evaluated at defined time points occurred without changes compared to the sham exposed samples (Figure 16). More in detail, cell cultures reached about 50% of closure after only 18h, thus showing the high capacity of MSC to proliferate after damage regardless of QMR treatment.

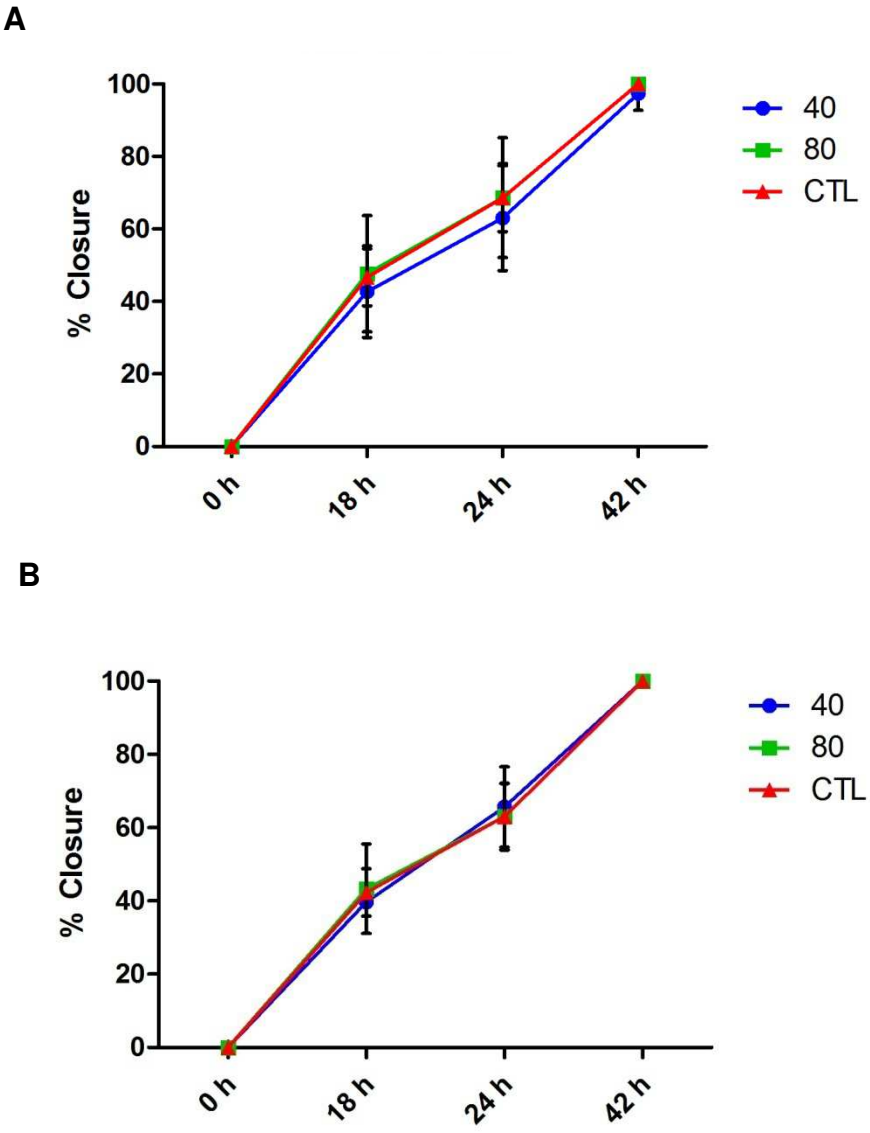

Figure 16. Scratch test migration assay. After the creation of a gap on a MSC monolayer, cell cultures were monitored at 0 h, 18 h, 24 h and 42 h. A) First cycle of treatment; B) Second cycle of treatment. Mean ± SD of n=3 independent experiments.

4.7 Microarray analysis

Based on previous results, we studied at a molecular level the effect of QMR on MSC performing microarray experiments after only 1 cycle of QMR treatment (Day 7).

Pre-processing microarray data analysis reduced the initial number of transcripts from 28000 to 12600. Thereafter, samples were grouped on the basis of the similarity of gene expression profiles (Figure 17). Results of clustering showed that samples grouped mainly according to the donor's provenience and not on the basis of QMR treatments, as a result of a inherent biological variability between analyzed MSC batches. Noteworthy, 3 out of 16 samples grouped independently of the MSC batch or QMR stimulation, due to an aberrant hybridization previously observed during pre-processing analysis (arrows in Figure 17).

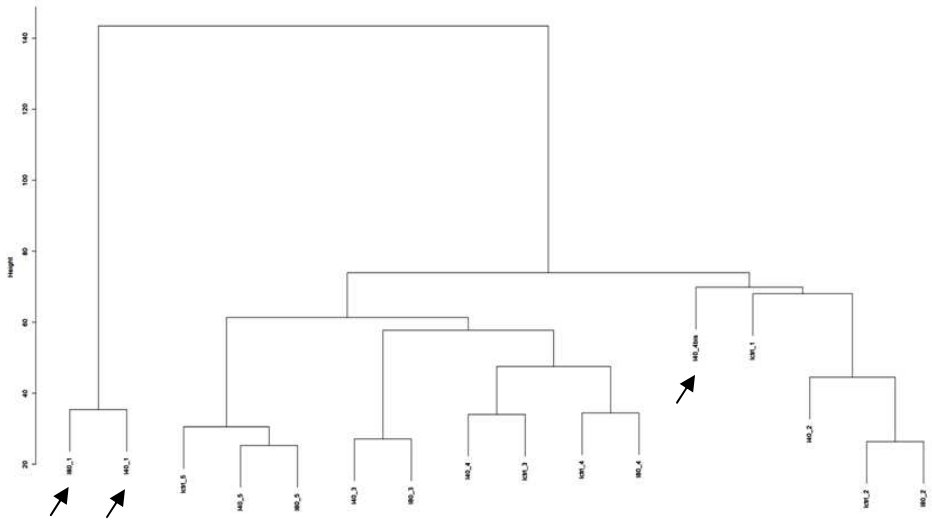

Figure 17. Clustering graphic of samples according to similarity of gene expression profiles. Image showing all the grouped samples after the pre-analysis: 4 clusters could be identified in relation to each MSC batch. The arrows indicate the aberrant hybridized samples.

The differentially expressed genes (DEG) analysis was employed to identify the differences between QMR-treated and sham-exposed MSC cultures (Table C). According to a cut-off p-value<0.05, 411 up-regulated and 987 down-regulated genes were found when using 40 as nominal power. At 80, 163 genes were found up-regulated while 199 down-regulated.

Comparison	N° up-regulated genes	Fold-change (max)	N° down-regulated genes	Fold-change (max)	p-value	Adjusted p-value
40 treatment vs control	411	2,5	987	2,3	<0,05	<0,496
80 treatment vs control	163	2,9	199	1,4	<0,05	<0,999

Table C. Up- and down- regulated genes associated with QMR treatment. The elaboration of the results was assessed by comparing QMR-treated MSC (after 1 cycle of QMR at 40 and 80 nominal powers) with untreated control cultures.

The best enrichment of gene lists was studied using ToppGene Suite and Ingenuity Pathway Analysis (IPA) softwares, to investigate the biological processes potentially associated with QMR stimulation. This approach allowed us to identify several cellular pathways involved in QMR and to restrict the number of genes for subsequent analysis. Noteworthy, the majority of genes had low values of significance (Figure 18). Up- and down-regulated genes at 40 nominal power were reduced of 61% and 66%, respectively. At 80, the majority (83%) of up-regulated and the 100% of down-regulated genes were not suitable for further analysis.

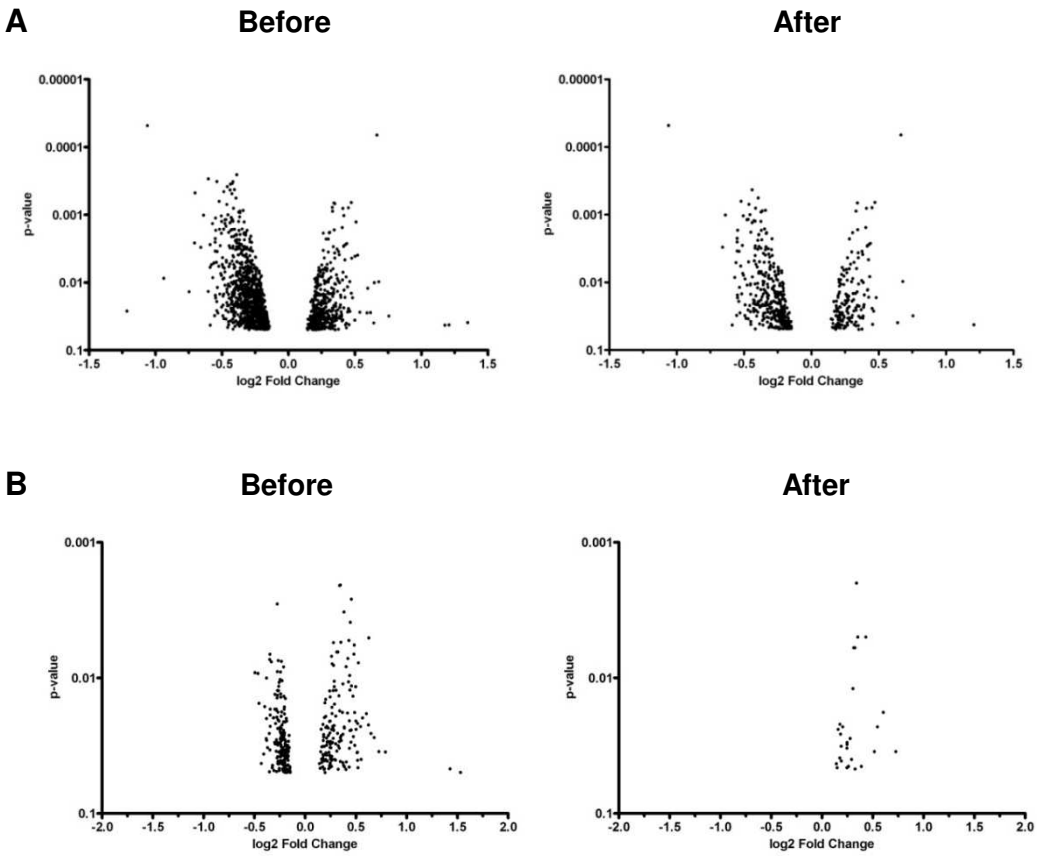

Figure 18. Dot plots of differentially expressed genes after QMR stimulation at 40 and 80 nominal powers. Images illustrated the distribution of (A) 40 and (B) 80 up- and down-regulated genes before and after the exclusion determined by the best enrichment of gene lists. The y-axis was in log10 scale.

As illustrated in Table D, 20 enrichment lists could be recognized associated with 40 nominal power (13 up-regulated and 7 down-regulated), while only 4 (all traceable to up-regulated genes) were found associated with 80. The main biological processes affected by QMR stimulation belonged to cellular, tissue and cardiovascular development categories. In particular, cellular development recurred in 40 and 80 dependent up-regulation and in 40 derived down-regulation.

Moreover, 2 arbitrary and more restrictive parameters were used for gene by gene analysis: a p-value ≤ 0.005 and a fold change ≥ 1.3. This more restrictive p-value implicated further reduction of more than 50% of the initial detected genes.

Category	N° lists	Changed genes	
		p≤0.05	p≤0.005
40 up-regulation	***13***	***114***	***18***
Cellular Development	2	42	11
Tissue Development	3	25	9
Cellular Differentiation	2	27	5
Cardiovascular Development	6	19	8
40 down-regulation	***7***	***152***	***50***
Phosphorylation	3	62	14
Cellular Development	2	110	38
Cellular Migration	1	61	26
Anchoring junction	1	16	5
80 up-regulation	***4***	***4***	***3***
Extracellular Matrix Organization	2	2	2
Cellular Development	2	2	1

Table D. Best enrichment gene lists. The best outcomes of ToppGene Suite and IPA softwares (FDR B&H q-value < 0.01 and B-H p-value < 0.01, respectively), considering fold changes ≥ 1.3, the number of changed genes with p-value ≤ 0.05 and arbitrary p-value ≤ 0.005, were illustrated.

The total number of modulated genes belonging to 40 dependent down-regulation (n=50) was bigger than the up-regulated condition (n=18), in contrast to the number of the relative total number of categories (n=13 for

40 up-regulation and n=7 for 40 down-regulation). These results were due to a redundancy of lots of genes. It was the case of genes like transcription and regulatory factors, phosphoproteins and kinases which are involved in multiple biological processes. Generally, 61% of 40 up-regulated genes and 44% of 40 down-regulated genes were annotated in regard only to an enrichment category.

Concerning 80 up-regulated genes, the application of more restrictive parameters did not significantly modify their number (from initial 4 genes to 3 final genes).

Finally, 8 differentially expressed genes after 40 QMR stimulation, considered the best genes in terms of significance, were in depth investigated in quantitative real time PCR (Table E). They were involved in biological processes related to cellular and tissue regeneration, like ECM remodeling, angiogenesis, cellular migration and regulation of actin filaments. Moreover, RUNX2 and SOX9, 2 genes involved in osteogenic and chondrogenic differentiation pathways were considered [62; 63].

By contrast, 3 differentially expressed genes obtained by 80 QMR treatment were not further investigated, due to the very low values compared to 40 setting.

Gene name	P-value	Fold change	Protein name	Function
MMP1	0,00007	1,6	Interstitial collagenase	Cleaves collagens of types I, II, and III
PLAT	0,003	1,4	Tissue-type plasminogen activator	Role in tissue remodeling
SLIT2	0,003	1,3	Slit homolog 2 protein	Molecular guidance in cellular migration
ARHGAP22	0,004	1,3	Rho GTPase-activating protein 22	Regulates endothelial cell capillary tube formation
A2M	0,00005	-2,1	Alpha-2-macroglobulin	Inhibitor of proteinases
CORO1B	0,001	-1,4	Coronin-1B	Regulates leading edge dynamics and cell motility
SHC1	0,002	-1,5	SHC-transforming protein 1	Signaling adapter
FN1	0,005	-1,4	Fibronectin	Involved in cell adhesion and motility
RUNX2	0,007	1,4	Runt-related transcription factor 2	Transcription factor involved in osteoblastic differentiation
SOX9	0,007	0,3	SRY-box 9	Regulates expression of genes involved in chondrogenesis

Table E. Selected genes for testing microarray outcomes in quantitative real time PCR. The individuated genes took part to biological processes where MSC could have a role in the regenerative support or differentiation after QMR stimulation.

4.8 Gene expression in quantitative real time PCR

Quantitative real time PCR was carried out after treating MSC cultures at 40 nominal power for 1 QMR cycle, to confirm the expression of 10 interesting genes, including 6 genes up-regulated (MMP1, PLAT, SLIT2, ARHGAP22, RUNX2 and SOX9) and 4 down-regulated (A2M, CORO1B, SHC1, FN1).

Our results, as shown in Figure 19, partially confirmed microarray results in gene expression. In particular MMP1, PLAT, ARHGAP22 and A2M revealed significant positive fold changes compared to the controls. By

contrast SLIT2, CORO1B, SHC1, FN1, RUNX2 and SOX9 were not found modulated by QMR treatment.

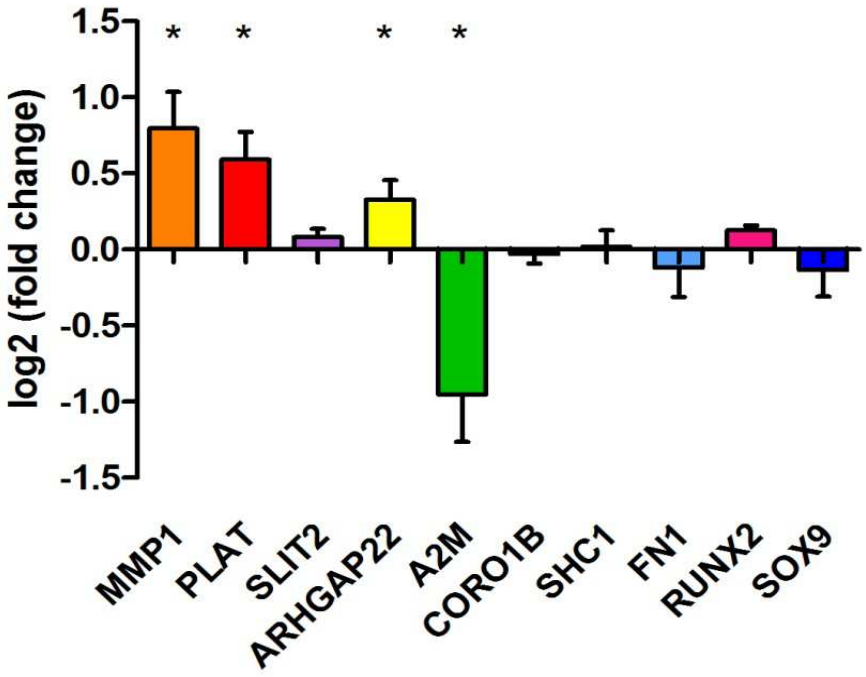

Figure 19. Fold changes in gene expressions using quantitative real time PCR. Expression of 10 genes selected by microarray was illustrated after n=4 independent experiments; mean ± SEM; * $p<0.05$.

5. Discussion

The present work was focused on understanding how QMR acts on human MSC. Actually, medical devices based on QMR are employed for the treatment of musculoskeletal disorders and post-surgical conditions [41; 42].

In our experimental setting we have evidenced that the treatment with QMR do not alter morphology and do not induce cell death on MSC.

Cellular proliferation and metabolic activity of treated cells were measured calculating population doubling at the end of each QMR cycle and by WST-1 assay respectively. Our data do not show any alteration of cellular proliferation or cellular metabolism after QMR stimulations.

It has been evidenced that EMFs and electric fields have the capacity to modify cell physiology and signaling pathways altering ion channels, transport protein activation and intracellular ionic concentration [4; 64]. In particular some results suggest that EMFs affect early stages of differentiation and reduce the time of differentiation [65; 66]. Moreover, Teven and colleagues [67] have demonstrated that high frequency pulsed EMF stimulation augmented osteogenic differentiation. We have observed that the ability of MSC exposed to QMR to generate mesodermal tissues (adipose tissue, bone, cartilage) was unaltered by the treatment. Data was confirmed in quantitative real time PCR by an unaltered expression of RUNX2 and SOX9, early molecular markers of osteogenesis and chondrogenesis differentiation respectively.

The typical markers expressed by MSC like CD90, CD105 and CD73 were not altered after QMR stimulation, suggesting that the treatment has no effect on cellular phenotype.

To investigate a possible effect of QMR at molecular level, we have performed gene expression profiling experiments. As expected for biological systems, microarray analysis revealed a high variability between the different MSC batches maybe explaining the observed functional differences between MSC subsets [68].

DEG analysis revealed that MSC exposed at 40 QMR setting had more regulated genes suggesting that treatment at this nominal power is more effective than 80 in inducing molecular changes.

The main biological processes affected by QMR stimulation revealed by functional analysis of gene lists [69; 70] belonged to development categories. In particular, 6 gene lists were related to cardiovascular development, cardiac differentiation and angiogenic response [14; 71].

Gene by gene analysis also revealed that up- and down-regulated genes were involved in cellular and tissue regeneration processes such as ECM remodeling, angiogenesis, cellular migration and regulation of actin filaments.

The most representative genes for each category were further validated in quantitative real time PCR on MSC exposed to 40 nominal power after a single QMR cycle. Overall, 40% of them comprising ARHGAP22, MMP1, PLAT and A2M showed statistical significance compared to controls.

ARHGAP22 is gene expressing a RhoGAP cytoplasmic protein involved in angiogenesis and in the negative regulation of rearrangement of actin filaments through the inhibition of Rac1 [72; 73]. This data is interesting

since some frequencies produced by QMR treatment are inside the endogenous range that affect actin and microtubule filaments [1].

Interestingly, up-regulated MMP1, PLAT and A2M genes are involved in the ECM remodeling through the fibrinolytic system that is also implicated in embryogenesis, wound healing and angiogenesis [74].

PLAT is a serine protease that converts plasminogen into plasmin where the latter activates other proteases including MMP1 [74]. Neuss and collaborators [75] demonstrated that MSC are able to secrete enzymes involved into this biological pathway and our results showed its promotion by stimulated MSC. In particular the positive regulation of the two enzymes PLAT (upstream protein) and MMP1 (downstream protein) was in perfect combination with the negative regulation of the inhibitor of proteases A2M.

Proteases participate in the regulation of angiogenesis through a modulation of an extremely complex process [76] whereas extracellular proteolysis is a requirement for new blood vessel formation. Therefore matrix metalloproteinases as well as plasminogen activator-plasmin systems play an important role during angiogenesis [77; 78].

Other studies demonstrated a direct induction of angiogenic factors using electric current [79-81] and our results suggest that QMR promotes low release and bioavailability of factors stored in ECM reservoir [82-84] without a concomitant increase in the expression of these stimulators. For example, PLAT is able to activate platelet-derived growth factor C (PDGF-C) [85].

In conclusion, our data suggests that in our model QMR-treated MSC maintained unaltered cell phenotype, migration capacity, cell

proliferation, cell metabolism and the ability of MSC to differentiate into bone, cartilage and adipose tissue.

Microarray analysis suggested that QMR treatment could improve angiogenesis and favor tissue regeneration probably through ECM remodeling. Further studies are needed to investigate the process at the protein level.

Acknowledgements

I'd like to thank my Supervisor, Prof.ssa Maria Teresa Conconi, for her fully availability and Dr. Giuseppe Astori, co-Supervisor and technical director of Advanced Cellular Therapy Laboratory (San Bortolo Hospital, Vicenza), for giving me the opportunity to see behind the scenes and to challenge myself.

I'd like to express gratitude to Ing. Gianantonio Pozzato, his collaborators and engineers for their intellectual incentive (and not only) and for great help with the prototype, fundamental in this research project. Moreover thanks to Dr.ssa Valentina Adami and Dr.ssa Pamela Gatto for their precious support in microarray experiments.

I can't miss Dr.ssa Martina Bernardi, Dr.ssa Katia Chieregato and Dr.ssa Denise Peserico for their support. Last but not least I'd like to really thank Dr.ssa Eliana Amati for her scientific and human contribution during these three years and for her critical revision of my thesis.

References

[1] Cifra M, Fields JZ and Farhadi A. Electromagnetic cellular interactions. Progress in Biophysics and Molecular Biology (2011); 105:223-246.

[2] Taghian T, Narmoneva DA and Kogan AB. Modulation of cell function by electric field: a high-resolution analysis. J. R. Soc. Interface (2015); 12: 20150153.

[3] Pilla A, Fitzsimmons R, Muehsam D, Wu J, Rohde C and Casper D. Electromagnetic fields as first messenger in biological signaling: Application to calmodulin-dependent signaling in tissue repair. Biochimica et Biophysica Acta (2011); 1810:1236–1245.

[4] Liu Q and Song B. Electric field regulated signaling pathways. The International Journal of Biochemistry & Cell Biology (2014); 55:264–268.

[5] Maswiwat K, Wachner D, Gimsa J. Effects of cell orientation and electric field frequency on the transmembrane potential induced in ellipsoidal cells. Bioelectrochemistry (2008); 74(1):130-41.

[6] Pall ML. Electromagnetic fields act via activation of voltage-gated calcium channels to produce beneficial or adverse effects. J. Cell Mol Med (2013); 17 (8):958-965.

[7] Lee Y and Famouri P. The movement of actin–myosin biomolecular linear motor under AC electric fields: an experimental study. Journal of Colloid and Interface Science (2013); 394:312–318.

[8] Barnes FS and Greenebaum B. Bioengineering and biophysical aspects of electromagnetic fields. Handbook of biological effects of electromagnetic fields. Third edition (2007) edited by Taylor & Francis Group.

[9] Messerli MA and Graham DM. Extracellular electrical fields direct wound healing and regeneration. Biol Bull (2011); 221: 79–92.

[10] Fan W, Qian F, Ma Q, Zhang P, Chen T, Chen C, Zhang Y, Deng P, Zhou Z and Yu Z. 50 Hz electromagnetic field exposure promotes proliferation and cytokine production of bone marrow mesenchymal stem cells. Int J Clin Exp Med (2015); 8(5):7394-7404.

[11] Zimmerman JW, Pennison MJ, Brezovich I, Yi N, Yang CT, Ramaker R, Absher D, Myers RM, Kuster N, Costa FP, Barbault A and Pasche B. Cancer cell proliferation is inhibited by specific modulation frequencies. British Journal of Cancer (2012); 106:307 – 313.

[12] Stacey M, Fox P, Buescher S and Kolb J. Nanosecond pulsed electric field induced cytoskeleton, nuclear membrane and telomere damage adversely impact cell survival. Bioelectrochemistry (2011); 82:131–134.

[13] Yoon YJ, Li G, Kim GC, Lee HJ and Song K. Effects of 60-Hz time-varying electric fields on DNA damage and cell viability support negligible genotoxicity of the electric fields. JEES (2015); 15(3):134-141.

[14] Serena E, Figallo E, Tandon N, Cannizzaro C, Gerecht S, Elvassore N and Vunjak-Novakovic G. Electrical stimulation of human embryonic stem cells: Cardiac differentiation and the generation of reactive oxygen species. Exp Cell Res. (2009); 315(20): 3611–3619.

[15] Rouabhia M, Park H, Meng S, Derbali H and Zhang Z. Electrical stimulation promotes wound healing by enhancing dermal fibroblast activity and promoting myofibroblast transdifferentiation. PLoS One (2013); 8(8): e71660.

[16] Maioli M, Rinaldi S, Santaniello S, Castagna A, Pigliaru G, Gualini S, Fontani V and Ventura C. Radiofrequency energy loop primes cardiac, neuronal, and skeletal muscle differentiation in mouse embryonic stem cells: a new tool for improving tissue regeneration. Cell Transplantation (2012); 21:1225–1233.

[17] Zhao Z, Watt C, Karystinou A, Roelofs AJ, McCaig CD, Gibson IR and De Bari C. Direct migration of human bone marrow mesenchymal stem cells in a physiology direct current electric field. European Cells and Materials (2011); 22:344-358.

[18] Tandon N, Goh B, Marsano A, Chao PG, Montouri-Sorrentino C, Gimble J and Vunjak-Novakovic G. Alignment and elongation of human

adipose-derived stem cells in response to direct-current electrical stimulation. Conf Proc IEEE Eng Med Biol Soc. (2009); 1: 6517–6521.

[19] Zhang J, Ren R, Luo X, Fan P, Liu X, et al. A small physiological electric field mediated responses of extravillous trophoblasts derived from HTR8/SVneo cells: involvement of activation of focal adhesion kinase signaling. PLoS ONE (2014); 9(3): e92252.

[20] Gomez-Ochoa I, Gomez-Ochoa P, Gomez-Casal F, Cativiela E and Larrad-Mur L. Pulsed electromagnetic fields decrease proinflammatory cytokine secretion (IL-1b and TNF-a) on human fibroblast-like cell culture. Rheumatol Int (2011); 31:1283–1289.

[21] Vianale G, Reale M, Amerlo P et al. Extremely low frequency electromagnetic field enhances human keratinocyte cell growth and decreases proinflammatory chemokine production. Br J Dermatol (2008); 158:1189-1196.

[22] Jennings J, Chen D and Feldman D. Transcriptional response of dermal fibroblasts in direct current electric fields. Bioelectromagnetics (2008); 29:394-405.

[23] Lee HC, Hong M, Jung SH, Kim BC, Suh YJ, Ko Y, Lee Y, Lee B, Cho Y, Myung S and Lee J. Effect of extremely low frequency magnetic fields on cell proliferation and gene expression. Bioelectromagnetics (2015); 36:506-516.

[24] Hess R, Neubert H, Seifert A, Bierbaum S, Hart DA and Scharnweber D. A novel approach for in vitro studies applying electrical fields to cell cultures by transformer-like coupling. Cell Biochem Biophys (2012); 64(3):223-32.

[25] Balint R, Cassidy NJ and Cartmel SH. Electrical stimulation: a novel tool for tissue engineering. Tissue Eng Part B Rev (2013); 19(1):48-57.

[26] Hernández-Bule ML, Paíno CL, Trillo MA and Úbeda A. Electric stimulation at 448 kHz promotes proliferation of human mesenchymal stem cells. Cell Physiol Biochem (2014); 34:1741-1755.

[27] Foster KR. Thermal and non-thermal mechanisms of interaction of radio-frequency energy with biological systems. IEEE Transactions on plasma science (2000); 28(1):15-23.

[28] Griffin M, Sebastian A, Colthurst J, and Bayat A. Enhancement of differentiation and mineralization of osteoblast-like cells by degenerate electrical waveform in an in vitro electrical stimulation model compared to capacitive coupling. PLoS ONE (2013); 8(9): e72978.

[29] Tepper OM, Callaghan MJ, Chang EI, Galiano RD, Bhatt KA, Baharestani S, Gan J, Simon B, Hopper RA, Levine JP and Gurtner GC. Electromagnetic fields increase in vitro and in vivo angiogenesis through endothelial release of FGF-2. FASEB J (2004); 18(11):1231-3.

[30] Markov MS. Expanding use of pulsed electromagnetic field therapies. Electromag Biol Med (2007); 26:257-274.

[31] Nuccitelli R. A role for endogenous electric fields in wound healing. Curr Top Dev Biol (2003); 58:1-26.

[32] Costin G, Birlea S and Norris D. Trends in wound repair: cellular and molecular basis of regenerative therapy using electromagnetic fields. Current Molecular Medicine (2012); 12:14-26.

[33] Todd DJ, Heylings DJ, Allen GE et al. Treatment of chronic varicose ulcers with pulsed electromagnetic fields: a controlled pilot study. Irmed J (1991); 84: 54-55.

[34] Canedo-Dorantes L, Garcia-Cantu R, Barrera R, et al. Healing of chronic arterial and venous leg ulcers through systemic electromagnetic fields. Arch Med Res (2002); 33: 281-289.

[35] Aleem IS, Aleem I, Evaniew N, Busse JW, Yaszemsk M, Agarwal A, Einhorn T and Bhandari M. Efficacy of electrical stimulators for bone healing: a meta-analysis of randomized sham-controlled trials. Sci Rep (2016); 6: 31724.

[36] Mayer-Wagner S, Passberger A, Sievers B, Aigner J, Summer B, Schiergens TS, Jansson V and Muller PE. Effects of low frequency electromagnetic fields on the chondrogenic differentiation of human mesenchymal stem cells. Bioelectromagnetics (2011); 32:283-290.

[37] Maziarz A, Kocan B, Bester M, Budzik S, Cholewa M, Ochiya T, Banas A. How electromagnetic fields can influence adult stem cells: positive and negative impacts. Stem Cell Res Ther (2016); 7(1):54.

[38] Pozzato G and Vignato G. Teoria della risonanza quantica molecolare nella realizzazione del bisturi elettronico "Vesalius". Quintessence International (2003); 5/6:153-155.

[39] D'Eredità R, Bozzola L. Molecular resonance vs. coblation tonsillectomy in children. Laryngoscope (2009); 119 (10): 1897-901.

[40] Schiavon M, Calabrese F, Nicotra S, Marulli G, Pozzato G, Giacometti C, Valente M and Rea F. Favorable tissue effects of quantum molecular resonance device (Vesalius) compared with standard electrocautery. A novel paradigm in lung surgery. Eur Surg Res (2007); 39: 222–228.

[41] Tröbinger V. Esperienza clinica nell'impiego del dispositivo Rexon-Age (2009).
http://teleamedical.com/telea2013/wp-content/uploads/fisioterapia-04.pdf

[42] Rossetti R. Risultati ottenuti in terapia antalgico-riabilitativa attraverso l'impiego del Rexon-age (2008).
http://teleamedical.com/telea2013/wp-content/uploads/fisioterapia-07.pdf

[43] Dal Maschio M, Canato M, Pigozzo FM, Cipullo A, Pozzato G and Reggiani C. Biophysical effects of high frequency electrical field (4-64 MHz) on muscle fibers in culture. Basic Applied Myology (2009); 19(1): 49-56.

[44] Dominici M, Le Blanc K, Mueller I, Slaper-Cortenbach I, Marini F, Krause D, Deans R, Keating A, Prockop D, Horwitz E. Minimal criteria for defining multipotent mesenchymal stromal cells. The International Society for Cellular Therapy position statement. Cytotherapy. (2006); 8(4):315-7.

[45] Keating A. Mesenchymal stromal cells: new directions. Cell Stem Cell (2012); 10 (6):709-16.

[46] Singer NG and Caplan AI. Mesenchymal stem cells: mechanisms of inflammation. Annu Rev Pathol (2011); 6:457-78.

[47] Park CW, Kim KS, Bae S, Son HK, Myung PK, Hong HJ, Kim H. Cytokine secretion profiling of human mesenchymal stem cells by antibody array. Int J Stem Cells (2009); 2(1):59-68.

[48] Boomsma RA, Geenen DL. Mesenchymal stem cells secrete multiple cytokines that promote angiogenesis and have contrasting effects on chemotaxis and apoptosis. PLoS One (2012);7(4):e35685.

[49] Ren G, Chen X, Dong F, Li W, Ren X, Zhang Y, Shi Y. Concise review: mesenchymal stem cells and translational medicine: emerging issues. Stem Cells Transl Med (2012); 1(1):51-8.

[50] Rennert RC, Sorkin M, Garg RK, Gurtner GC. Stem cell recruitment after injury: lessons for regenerative medicine. Regen Med (2012); 7(6):833-50.

[51] Krampera M. Mesenchymal stromal cell 'licensing': a multistep process. Leukemia (2011); 25: 1408–1414.

[52] Kasper G, Dankert N, Tuischer J, Hoeft M, Gaber T, Glaeser JD, Zander D, Tschirschmann M, Thompson M, Matziolis G, Duda GN. Mesenchymal stem cells regulate angiogenesis according to their mechanical environment. Stem Cells (2007); 25(4):903-10.

[53] Murphy MB, Moncivais K, Caplan AI. Mesenchymal stem cells: environmentally responsive therapeutics for regenerative medicine. Exp Mol Med (2013); 45:e54.

[54] Maxson S, Lopez EA, Yoo D, Danilkovitch-Miagkova A, Leroux MA. Concise review: role of mesenchymal stem cells in wound repair. Stem Cells Transl Med (2012); 1(2):142-9.

[55] Badiavas EV, Falanga V. Treatment of chronic wounds with bone marrow-derived cells. Arch Dermatol (2003); 139:510 –516.

[56] Dash NR, Dash SN, Routray P et al. Targeting non healing ulcers of lower extremity in human through autologous bone marrow-derived mesenchymal stem cells. Rejuvenation Res (2009); 12:359 –366.

[57] Chen Y, Xiang LX, Shao JZ, et al. Recruitment of endogenous bone marrow mesenchymal stem cells towards injured liver. J Cell Mol Med (2010); 14(6B):1494–1508.

[58] Berridge MV, Herst PM, Tan AS. Tetrazolium dyes as tools in cell biology: new insights into their cellular reduction. Biotechnol Annu Rev (2005); 11:127-52.

[59] Ritchie ME, Phipson B, Wu D, Hu Y, Law CW, Shi W, Smyth GK. limma powers differential expression analyses for RNA-sequencing and microarray studies. Nucleic Acids Res (2015); 43(7):e47.

[60] Analysis of relative gene expression data using real-time quantitative PCR and the 2(-Delta Delta C(T)) Method. Livak KJ, Schmittgen TD. Methods (2001); 25(4):402-8.

[61] Ragni E, Viganò M, Rebulla P, Giordano R, Lazzari L. What is beyond a qRT-PCR study on mesenchymal stem cell differentiation properties: how to choose the most reliable housekeeping genes. J Cell Mol Med (2013); 17(1):168-80.

[62] Ross CL, Siriwardane M, Almeida-Porada G, Porada CD, Brink P, Christ GJ, Harrison BS. The effect of low-frequency electromagnetic field on human bone marrow stem/progenitor cell differentiation. Stem Cell Res (2015); 15(1):96-108.

[63] Mardani M, Roshankhah S, Hashemibeni B, Salahshoor M, Naghsh E and Esfandiari E. Induction of chondrogenic differentiation of human adipose-derived stem cells by low frequency electric field. Adv Biomed Res (2016); 5:97.

[64] Sundelacruz S, Levin M and Kaplan DL. Membrane potential controls adipogenic and osteogenic differentiation of mesenchymal stem cells. PLoS One (2008); 3(11):e3737.

[65] Sun LY, Hsieh DK, Lin PC, Chiu HT, Chiou TW. Pulsed electromagnetic fields accelerate proliferation and osteogenic gene expression in human bone marrow mesenchymal stem cells during osteogenic differentiation. Bioelectromagnetics (2010); 31:209–19.

[66] Esposito M, Lucariello A, Riccio I, Riccio V, Esposito V, Riccardi G. Differentiation of human osteoprogenitor cells increases after treatment with pulsed electromagnetic fields. In Vivo (2012); 26:299–304.

[67] Teven CM, Greives M, Natale RB, Su Y, Luo Q, He BC, Shenaq D, He TC, Reid RR. Differentiation of osteoprogenitor cells is induced by high-frequency pulsed electromagnetic fields. J Craniofac Surg (2012); 23(2):586-93.

[68] Tormin A, Brune JC, Olsson E, Valcich J, Neuman U, Olofsson T, Jacobsen SE, Scheding S. Characterization of bone marrow-derived mesenchymal stromal cells (MSC) based on gene expression profiling of functionally defined MSC subsets. Cytotherapy (2009); 11(2):114-28.

[69] Huang DW, Sherman BT and Lempicki RA. Bioinformatics enrichment tools: paths toward the comprehensive functional analysis of large gene lists. Nucleic Acids Research (2009); 37(1):1–13.

[70] Collard JF and Hinsenkamp M. Cellular processes involved in human epidermal cells exposed to extremely low frequency electric fields. Cell Signal (2015); 27(5):889-98.

[71] Sheikh AQ, Taghian T, Hemingway B, Cho H, Kogan AB, Narmoneva DA. Regulation of endothelial MAPK/ERK signalling and capillary morphogenesis by low-amplitude electric field. J R Soc Interface (2013); 10(78):20120548.

[72] Marinković G, Heemskerk N, van Buul JD, de Waard V. The Ins and Outs of Small GTPase Rac1 in the Vasculature. J Pharmacol Exp Ther (2015); 354(2):91-102.

[73] Mori M, Saito K and Ohta Y. ARHGAP22 localizes at endosomes and regulates actin cytoskeleton. PLoS One (2014); 9(6):e100271.

[74] Heissig B, Dhahri D, Eiamboonsert S, Salama Y, Shimazu H, Munakata S, Hattori K. Role of mesenchymal stem cell-derived fibrinolytic factor in tissue regeneration and cancer progression. Cell Mol Life Sci (2015); 72(24):4759-70.

[75] Neuss S, Schneider RK, Tietze L, Knüchel R, Jahnen-Dechent W. Secretion of fibrinolytic enzymes facilitates human mesenchymal stem cell invasion into fibrin clots. Cells Tissues Organs (2010); 191(1):36-46.

[76] Roy R, Zhang B and Moses MA. Making the cut: protease-mediated regulation of angiogenesis. Experimental Cell Research (2006); 312:608-622.

[77] Pepper MS. Role of the matrix metalloproteinase and plasminogen activator-plasmin systems in angiogenesis. Arterioscler Thromb Vasc Biol (2001); 21(7):1104-17.

[78] Nam HS, Kwon I, Lee BH, Kim H, Kim J, An S, Lee OH, Lee PH, Kim HO, Namgoong H, Kim YD and Heo JH. Effects of mesenchymal stem cell treatment on the expression of matrix metalloproteinases and angiogenesis during ischemic stroke recovery. PLoS One (2015); 10(12):e0144218.

[79] Kim IS, Song JK, Zhang YL, Lee TH, Cho TH, Song YM, Kim DK, Kim SJ, Hwang SJ. Biphasic electric current stimulates proliferation and induces VEGF production in osteoblasts. Biochim Biophys Acta (2006); 1763(9):907-16.

[80] Bai H, Forrester JV and Zhao M. DC electric stimulation up-regulates angiogenic factors in endothelial cells through activation of VEGF receptors. Cytokine (2011); 55(1):110-5.

[81] Asadi MR, Torkaman G, Hedayati M and Mofid M. Role of sensory and motor intensity of electrical stimulation on fibroblastic growth factor-2 expression, inflammation, vascularization, and mechanical strength of full-thickness wounds. J Rehabil Res Dev (2013); 50(4):489-98.

[82] Park JE, Keller GA and Ferrara N. The vascular endothelial growth factor (VEGF) isoforms: differential deposition into the subepithelial

extracellular matrix and bioactivity of extracellular matrix-bound VEGF. Mol. Biol. Cell (1993); 4:1317– 1326.

[83] Whitelock JM, Murdoch AD and Iozzo RV. The degradation of human endothelial cell-derived perlecan and release of bound basic fibroblast growth factor by stromelysin, collagenase, plasmin and heparanases. J Biol Chem (1996); 271:10079–10086.

[84] Bonnans C, Chou J, Werb Z. Remodelling the extracellular matrix in development and disease. Nat Rev Mol Cell Biol (2014); 15(12):786-801.

[85] Fredriksson L, Li H, Fieber C, Li X and Eriksson U. Tissue plasminogen activator is a potent activator of PDGF-CC. EMBO J (2004); 23(19):3793-802.